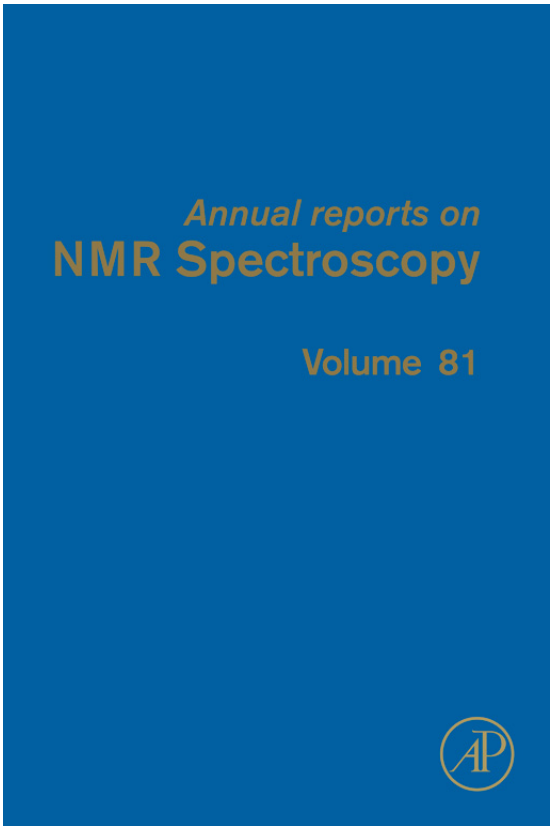

From: Pedro Salvador, Dependencies of *J*-Couplings upon Dihedral Angles on Proteins. In Graham A. Webb, editor:
Annual Reports On NMR Spectroscopy, Vol. 81,
Burlington: Academic Press, 2014, pp. 185-227.
ISBN: 978-0-12-800185-1

CHAPTER FIVE

Dependencies of *J*-Couplings upon Dihedral Angles on Proteins

Pedro Salvador
Institut de Química Computacional i Catàlisi, Universitat de Girona, Girona, Spain

Contents

Abstract

Indirect spin–spin coupling constants, or simply *J*-couplings, are one of the most useful and widely used NMR parameters for structure determination. Accurate analytic representation of their structural dependence is crucial for quantitative analysis. The dependence of vicinal *J*-coupling constants upon the dihedral angle of the coupled nuclei was first established by Karplus more than 50 years ago. Since then, Karplus original equations have been extensively modified and generalized in order to account for different effects upon the *J*-coupling values.

In this work, we critically analyse the use of such Karplus-type equations for the description of the dihedral dependence of *J*-couplings derived from both experiment and first principles. The use of alternative nonanalytic expressions is also discussed. Finally, we have collected the most accurate *J*-coupling parameterizations of the recent literature, particularly those that exhibit explicit dependence upon the dihedral angles that govern the backbone and side-chain conformations of polypeptide chains.

Key Words: *J*-coupling, Indirect spin–spin coupling, Karplus equation, Structure determination, Phi/psi dihedral angles

Annual Reports on NMR Spectroscopy, Volume 81
ISSN 0066-4103
http://dx.doi.org/10.1016/B978-0-12-800185-1.00005-X

1. INTRODUCTION

NMR spectroscopy has been revealed over more than 50 years as the most powerful technique for examining conformation of both organic and inorganic or organometallic compounds. The advent of high- and ultra-high-NMR spectrometers, the successive improvements in 2D, 3D, or 4D techniques, and the advances in molecular biology for ^{13}C and ^{15}N isotopic enrichment of biomolecules allow nowadays for the elucidation of the structure and dynamics of biological systems such as proteins, RNA, DNA, and carbohydrates.

Among the different types of NMR data that can be gathered in solution, namely, chemical shifts, NOE cross peaks, and residual dipolar couplings (RDCs), indirect nuclear spin–spin coupling constants, or simply *J*-couplings, represent a unique source of information for structure determination. Moreover, the measurement of *J*-couplings through hydrogen bonds has provided direct evidence of their presence, also allowing for the characterization of the hydrogen bond topology and local structural and electronic details.

NMR analysis of molecular geometry bids for accurate parameterization of the dependencies of *J*-coupling constants upon geometric parameters, such as bond distances, angles, and particularly dihedral angles.

Explicit dependence of the *J*-couplings on dihedral angles is typically established by using (fitting to) analytic expressions. Chiefly, this permits the derivation of the corresponding torsion angles from the value of the *J*-coupling constant for molecular structure analysis. However, the inverse function is multiple-valued (i.e. several dihedral angles conform to a typical value of a *J*-coupling) so that a second *J*-coupling that is dependent upon the same torsion angle may be necessary to solve the ambiguity. Different parameterizations of the same *J*-coupling may lead to differences of ca. 1 Hz [1], way over the accuracy of the present measurements. It may be argued that the *J*-couplings are less helpful than other NMR data for full, quantitative structure analysis. See, however, recent successful applications by van Gunsteren [2].

In 1959, Karplus [3] described for the first time, and on theoretical grounds, the dependence of vicinal *J*-coupling constants upon the dihedral angle of the coupled protons in ethane as

$$ {}^{3}J_{\mathrm{H,H}} = \left.\begin{array}{ll} 8.5\,\cos^2\theta - 0.28 & 0 \le \theta \le \pi/2 \\ 9.5\,\cos^2\theta - 0.28 & \pi/2 \le \theta \le \pi/2 \end{array}\right\} \qquad (5.1) $$

In a subsequent paper [4], partially motivated by some criticism on the limitation of the theory, Karplus analysed the effect of the substituent's electronegativity and the dependence upon the bond angle and lengths (the latter turned out to be of minor relevance). On the basis of valence-bond arguments [5], Karplus introduced is most celebrated general equation for the dependence of the vicinal *J*-couplings on the dihedral angle, in the form of a series of (real) Fourier coefficients truncated after the third term:

$$J(\theta) = C_0 + C_1 \cos\theta + C_2 \cos 2\theta \tag{5.2}$$

where C_0, C_1, and C_2 are real constants. According to Karplus, such expression primarily suggests the expected trends on the basis of theoretical grounds and should be regarded as a zeroth-order approximation. Nevertheless, Eq. (5.2) or the most generally used form as a truncated cosine power series

$$J(\theta) = A \cos^2(\theta) + B\cos(\theta) + C \tag{5.3}$$

has had a pivotal role since then in the development of new and more accurate parameterizations of the dependence of *J*-couplings upon the molecular geometry.

The original Karplus equation has been subjected to continuous modifications and reparameterizations in order to embrace a vast number of different nuclear pairs on different molecular environments [6–23]. The scope of this chapter is to discuss the use of Karplus-type equations for the description of the dihedral dependence of *J*-couplings and to gather the most relevant data available to date, specifically devoted to the characterization of backbone (secondary structure) and side-chain conformations of proteins. *J*-couplings over one (^1J) and two (^2J) bond ones are not as highly used as the ^3J-couplings for structural determination, but notable exceptions will also be covered.

2. DETERMINATION OF KARPLUS PARAMETERS: FROM STATIC TO SELF-CONSISTENT FITTINGS

The parameters for the Karplus-type parameterizations are often determined empirically. In that case, it is essential to have accurate values of both the experimentally measured *J*-couplings and the corresponding relevant dihedral angles.

It is important to note that the measured *J*-couplings are a time average of instantaneous values, which are affected by the angular fluctuations of the

dihedral angles over a timescale of milliseconds [24]. In the *static* or *rigid* approach, one uses an individual structure that represents the averaged dihedral angles (either from an X-ray diffraction structure or from NMR data), and the motional averaging effects are automatically included in the adjusted coefficients during the parameterization process. For instance, a given *J*-coupling measured in solution is associated to a particular dihedral angle derived from an X-ray diffraction structure of the molecule in the crystal form. By using a sufficiently large number of *J*-couplings involving the same type of atoms (and often the same or very similar chemical environment), a set of parameters can be derived with appropriate statistical tools, usually the least squares minimization of the difference between the measured and the recalculated *J*-coupling values. A problem associated to the use of X-ray-derived structures is that one tacitly assumes that the geometry, in particular the torsional angle, in the crystal structure and in the solution is the same. Another issue is that in X-ray structures, the hydrogen atoms are typically added at idealized positions (e.g. assuming ideal tetrahedral geometries of the C^{α} atoms and perfect in-plane H^{N} positions in peptides). This introduces uncertainties in the dihedral angles involving proton positions. For instance, the difference in the H^{N}–N–C^{α}–H^{α} dihedral angles (see Fig. 5.1) in a high-resolution X-ray structure of GB3 [25] and a dipolar coupling-refined NMR structure [26] amounts to ca. 6.5° on average, more than twice the average deviation on the backbone torsion angles involving C atoms [24].

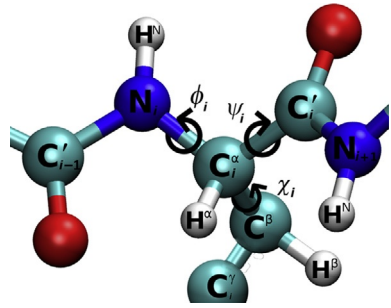

Figure 5.1 Labelling of the relevant atoms of a polypeptide chain. Subscripts i, $i-1$, and $i+1$ denote the current, preceding, and following residues in the sequence. Dihedral angles associated to the backbone $\phi(C'_{i-1}\text{–}N\text{–}C^{\alpha}\text{–}C'_i)$ and $\psi(N_i\text{–}C^{\alpha}\text{–}C'\text{–}N_{i+1})$ angles and to the side-chain torsion angle $\chi(N\text{–}C^{\alpha}\text{–}C^{\beta}\text{–}C^{\gamma})$ of the central residue are also depicted.

For a more appropriate interpretation of the experimental data, conformational flexibility must be taken into account. The experimental *J*-coupling values can be regarded as weighted average of the different dihedral angle "states":

$$\langle J \rangle \equiv \int p(\theta) J(\theta) \mathrm{d}\theta, \tag{5.4}$$

where $p(\theta)$ is the dihedral angle distribution function over the $[0,2\pi]$ range, assumed to follow a Gaussian normal distribution [27]. Harmonic motion can be included to the Karplus fits by considering an additional width parameter (σ) associated to the standard deviation of the dihedral angle over its average value. In such approach taking care of the *motion*, one can obtain appropriately modified Karplus coefficients [28] as

$$\langle J(\theta,\sigma) \rangle = A\mathrm{e}^{-2\sigma^2}\cos^2(\theta) + B\mathrm{e}^{-2\sigma^2}\cos(\theta) + \frac{A}{2}\left(1-\mathrm{e}^{-2\sigma^2}\right) + C \tag{5.5}$$

where $A' = A\mathrm{e}^{-2\sigma^2}$, $B' = B\mathrm{e}^{-2\sigma^2}$, and $C' = \frac{A}{2}\left(1-\mathrm{e}^{-2\sigma^2}\right) + C$. Moreover, the previous equation also suggests that a set of A, B, C parameters free from harmonic motion can be derived from the value of σ.

When motion effects are expected to be due to the existence of different conformations (multiple rotameric states significantly populated), rather to local fluctuations, they can also be accounted for with staggered-rotamer models [29], in which discrete probabilities for the different conformers are introduced. They are often used when describing amino acid side-chain torsion conformations. See, for instance, Ref. [30] for a recent critical analysis of several models.

The *J*-couplings may also be associated to an *ensemble* of structures derived from molecular dynamics (MD) simulations. The measured *J*-couplings are then fitted to the calculated values, which are averaged over the ensemble of structures:

$$\langle J_{\mathrm{calc}} \rangle = \sum_{k}^{M} J_{\mathrm{calc},k} \tag{5.6}$$

Sufficient conformational sampling and high-quality force fields, combined with more involved Karplus-type parameterizations, are required to derive accurate models to reproduce *J*-coupling measures from MD simulations. The accuracy obtained is often not too satisfactory [31].

Other techniques combine MD simulations techniques with appropriate restrains to conform to the NMR data such as NOEs, order parameters, RDCs, or *J*-couplings themselves. For instance, the dynamic ensemble refinement method [32] yields a set of conformations that conform to both the average structure and the fluctuations. Other approaches are applied by Clore and Schwieters [33,34].

Apparently, better reproduction of the *J*-coupling dependence upon dihedral angles is obtained when fitting the experimental couplings to dynamic ensemble NMR structures. The typical observation is that the Karplus-type equations exhibit larger variations as a function of the associated dihedral angle when they are derived from an ensemble of structures, as compared to those obtained from a single, averaged, dihedral angle (from either MD simulations or NMR or X-ray structures) [35]. Such ensemble-derived Karplus parameters are also closer to those obtained from first-principle electronic structure calculations [36].

Nowadays, many electronic structure codes include efficient implementations [37–41] of the Ramsey equations [42] for the calculations of nonrelativistic spin–spin coupling constants. A vast number of publications devoted to the calculation of *J*-couplings can be found in the literature, covering different aspects such as the basis set effects [43–55], the comparison of wave function versus density functional theory (DFT) methods [56–60], or the choice of exchange–correlation functional in DFT approaches [61–68]. Excellent recent reviews of Contreras [69] and Helgaker [70] cover these particular aspects.

Indeed, *ab initio* electronic structure methods permit the routine calculation of *J*-couplings for any nuclear configuration of the system, that is, free from molecular motion effects. They can also be readily used to explore the dependence of the *J*-coupling values upon other geometric parameters such as bond distances and bond angles, as well as electronic effects [71]. Several techniques have also been developed to assist in the rationalization and interpretation of the *J*-coupling values. Electron delocalization is the key factor for the transmission of the *J*-couplings, and conjugation, hyperconjugation, and charge–transfer effects are responsible for the enhancement (or the decrease) of the spin–spin coupling. Contreras *et al.* have devised a number of rules [71–76] for the rationalization of the values of one- and two-bond *J*-couplings in such terms.

The increase on the computational resources and the efficient implementation on electronic structure codes of the *J*-coupling calculations have already reached the point in which direct calculation of the *J*-couplings

(at least the leading Fermi contact contribution) along thousands of snapshots has replaced Karplus parameterizations for the assessment of dynamics effects on *J*-couplings in proteins [77,78]. Another recent example is the so-called automatic fragmentation quantum mechanics/molecular mechanics approach of Xiao [79]. In a most recent study [80], the authors applied the method to calculate at the PW91/IGLO-III level of theory $^3J(H^N,H^\alpha)$, $^3J(H^N,C^\beta)$, and $^3J(H^N,C')$ coupling for protein GB3 including dynamic effects. It was found that this direct approach yielded better agreement with experimental values than the available Karplus equations.

Last but not least, an interesting strategy proposed by Schmidt [81–83] exploits the redundant information given by the set of different *J*-couplings related to the *same* dihedral angle to obtain reliable Karplus coefficients without making explicit use of structural reference data from X-ray or NMR. For instance, in polypeptides, up to six measurable ^3J-couplings are associated to the same backbone torsion angle ϕ of a given residue, namely, $^3J(C'_{i-1},C'_i)$, $^3J(C'_{i-1},H^\alpha)$, $^3J(C'_{i-1},C^\beta)$, $^3J(H^N,H^\alpha)$, $^3J(H^N,C^\beta)$, and $^3J(H^N,C'_i)$. The dihedral angle is defined from the three-bond path $\phi_i(C'_{i-1}–N–C^\alpha–C'_i)$, as shown in Fig. 5.2. Thus, the $^3J(C'_{i-1},C'_i)$ coupling has a natural dependence upon ϕ. According to Karplus theory, the dependence of $^3J(C'_{i-1},C'_i)$ can be described by Eq. (5.3) where $\theta=\phi$. If perfect trigonal, planar, and tetrahedral geometries for the backbone N and C_α atom are assumed, the dependence of the remaining five ^3J-couplings upon the dihedral angle can be written using Eq. (5.3) making explicit reference to the same torsion angle by taking $\theta=\phi+\delta\phi$, where the torsion phase $\delta\phi$ depends upon the particular ^3J-coupling, as shown in Table 5.1.

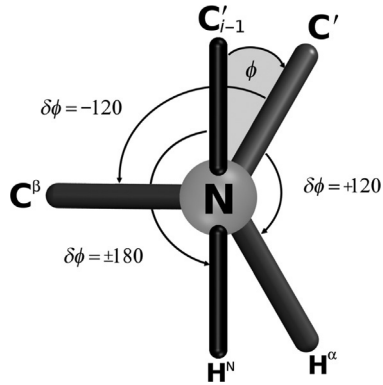

Figure 5.2 Newman projection of the peptide torsion angle $\phi_i(C'_{i-1}–N–C^\alpha–C'_i)$. Dihedral angle increments $\delta\phi$ are used to relate ϕ to alternative dihedral angles.

Table 5.1 Torsion phase angles used to relate ^3J-couplings to the definition of the dihedral backbone angle ϕ, according to IUPAC/IUB definition [84]

Coupling	Torsion phase ($\delta\phi$) (°)
$^3J(C'_{i-1},C'_i)$	0
$^3J(C'_{i-1},H^{\alpha})$	+120
$^3J(C'_{i-1},C^{\beta})$	−120
$^3J(H^N,H^{\alpha})$	−60
$^3J(H^N,C^{\beta})$	+60
$^3J(H^N,C'_i)$	±180

If a sufficient set of experimental ^3J-couplings are known for a protein (at least four couplings per residue in the particular case described), the whole set of experimental coupling constants can be used to adjust, simultaneously, a set of 18 Karplus parameters – three for each different type of ^3J-coupling, assuming the parametric dependence of Eq. (5.3) – *and* the unknown dihedral angles associated to each residue. Thus, in this so-called self-consistent fitting, the Karplus coefficients are not influenced by the differences between the solution and crystal states. Moreover, additional parameters for each residue such as Gaussian width parameters or rotamer probabilities can be included to explicitly account for angular motion in the fitting [82,83]. Extra dihedral angle parameters accounting for possible distortions of ideal bond geometries can also be included, though their effect was already found to be negligible [81]. Alternative extended Karplus equations including more parameters can also be used to improve the fitting process at the expense of a few more degrees of freedom in more complicated cases such as side-chain dihedral angles [82,83].

This promising method is expected to benefit in the near future from the collection of extensive sets of experimental *J*-couplings. Self-consistent corefinement using similar data from several proteins can enable to establish unique *J*-couplings dependencies of wider applicability. Whether measured ^1J- and ^2J-couplings exhibiting marked (and quantifiable) dependence upon dihedral angles can be combined with the ^3J ones is yet to be explored.

It is clear that in order *J*-couplings to be really useful for structure determination, it is critical to have at one disposal as accurate as possible analytic representations of their structural dependence. As mentioned earlier, Karplus original equations have been extensively modified and generalized in order to include different effects upon the *J*-coupling values, other than

the merely geometric ones. For the simplest of case of proton–proton vicinal ^3J(H,H) couplings in substituted ethanes (e.g. across H—C—C—H bonding paths), Haasnoot and Altona derived in the 1980s a number of a generalized Karplus parameterizations to account for the electronegativity of the substituents and their orientation [10–16], even including their nonadditive interactions in their actual most accurate versions [17]. Imai and Osawa introduced [22,23] a generalization of the Karplus equation including 22 adjustable parameters, incorporating explicit dependence on the C—C—H bond angles and C—C distances and on electronegativity/orientation of substituents. For an extensive coverage of the vast number of Karplus-type parameterizations of vicinal couplings on carbohydrates, see the recent review of Coxon [85]. In this sense, it is somewhat surprising that the well-known online calculation of homo- and heteronuclear ^3J-couplings for carbohydrates, nucleotides, and peptides of Stenutz [86] is still relying on Karplus-type parameterizations derived way before year 2000 (with two notable exceptions from Zhao [87] and Coxon [88] from 2007).

This work aims at collecting the most accurate *J*-coupling parameterizations of the recent literature, particularly those that are most relevant for protein structure determination. In the following, we will describe the most common analytic expressions used to describe the dependence of the *J*-couplings upon dihedral angles.

3. *J*-COUPLING DEPENDENCE UPON DIHEDRAL ANGLES

3.1. Analytic Expressions

A number of analytic expressions have been used in the literature to express the dependence of the *J*-couplings upon (mostly) dihedral angles. Karplus theory of vicinal coupling constants is simply expressed by Eqs. (5.2) or (5.3). The physical significance of the two sets of parameters, namely, (C_0, C_1, C_2) of Eq. (5.2) and (A, B, C) of Eq. (5.3), is represented in Figs. 5.3 and 5.4.

The Fourier-type parameterization of Eq. (5.2) is interesting as it collects the average value of the coupling magnitude in the independent coefficient C_0, as the average of the $\cos(n\theta)$ terms over the $[0,2\pi]$ interval vanishes. The primary and secondary maxima of the Karplus curve, that is, *trans* and *cis* orientations of the dihedral angle θ, respectively, differ by $2C_1$ (usually with negative value). The largest difference in the *J*-coupling value from its mean is related to the difference $(C_2 - C_1)$. See figure for more relationships.

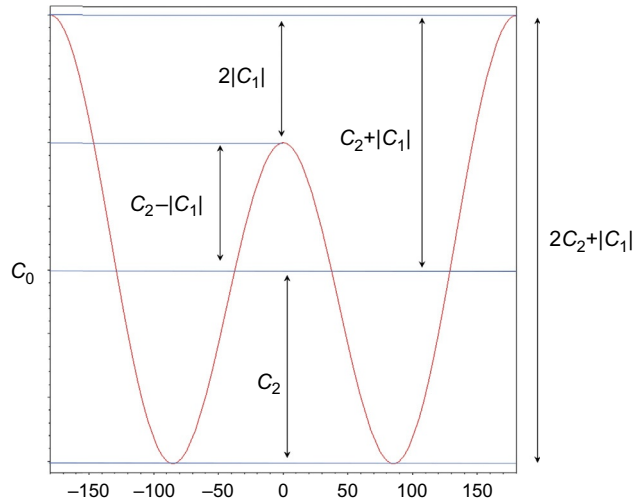

Figure 5.3 Physical interpretation of the Karplus coefficients of an equation of the form $J(\theta) = C_0 + C_1 \cos\theta + C_2 \cos 2\theta$. The parameter C_1 is assumed to be negative in this picture.

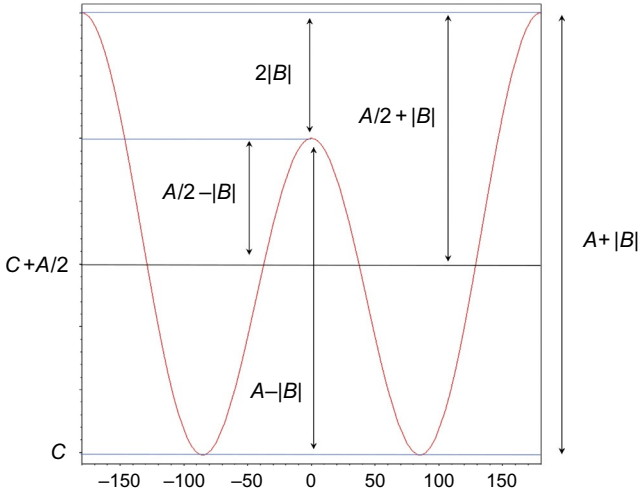

Figure 5.4 Physical interpretation of the Karplus coefficients of an equation of the form $J(\theta) = A \cos^2(\theta) + B \cos(\theta) + C$. The parameter B is assumed to be negative in this picture.

The most straightforward generalization of Eq. (5.2) is to consider a larger expansion of the Fourier series as

$$J(\theta) = \sum_k C_k \cos(k\theta) \tag{5.7}$$

Terms for $k=3$ are included in the parameterizations of Imai [22], Altona [14], and Tvaroška [89], among others. A recent parameterization of vicinal *J*-couplings for methionine methyl groups with DFT calculations made use of terms up to $k=6$ [90].

The main role of a $\cos(3\theta)$ term is to shift the maxima of $J(\theta)$ away from the $\theta = \pm\pi$ values, as illustrated in Fig. 5.5.

The relative height of the maxima at $\theta = 0$ and $\theta = \pm\pi$ is reversed if $|C_3| > |C_1|$. On the other hand, if $|C_3| > |C_1|$ but C_3 is also negative (we are considering the most typical case where C_1 is negative), the height of the maximum at $\theta = 0$ decreases, eventually leading to two maxima

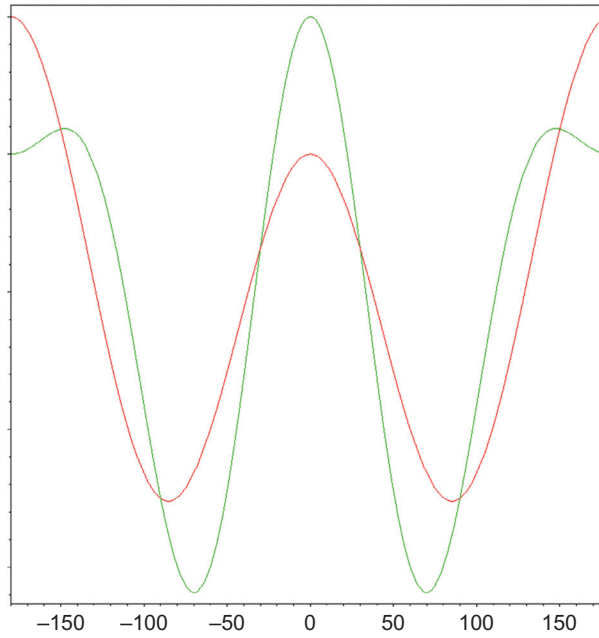

Figure 5.5 Comparison of the Karplus-type $J(\theta) = C_0 + C_1 \cos\theta + C_2 \cos 2\theta$ (red) and the extended $J(\theta) = C_0 + C_1 \cos\theta + C_2 \cos 2\theta + C_3 \cos 3\theta$ (green) equations. The parameter C_1 is assumed negative and $C_3 > 2|C_1|$.

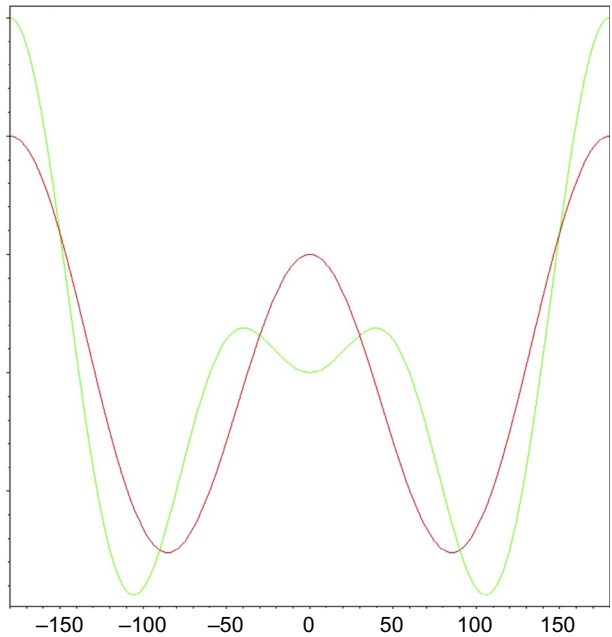

Figure 5.6 Comparison of the Karplus-type $J(\theta) = C_0 + C_1 \cos\theta + C_2 \cos 2\theta$ (red) and the extended $J(\theta) = C_0 + C_1 \cos\theta + C_2 \cos 2\theta + C_3 \cos 3\theta$ (green) equations. The parameters C_1 and C_3 are assumed negative and $|C_3| > 2|C_1|$.

symmetrically placed around the $\theta = 0$ value (see Fig. 5.6). In any case, the symmetry around the $\theta = 0$ value is still conserved, so the inclusion of higher-order $\cos(k\theta)$ terms for $k = 2, 3$, etc. in the analytic expression cannot account for asymmetries of the curve with respect to $\theta = 0$.

Asymmetry of the curve around $\theta = 0$ is simply achieved by adding extra $\sin(\theta)$ term to the to the original Karplus equation to get

$$J(\theta) = C_0 + C_1 \cos(\theta) + C_2 \cos(2\theta) + S_1 \sin(\theta) \tag{5.8}$$

As illustrated in Fig. 5.7, the difference of the values of the function at the minima in $\theta = -\pi/2$ and $\theta = +\pi/2$ is given by twice the value of the S_1 parameter.

The inclusion of sine terms was first proposed by Pachler [8] in order to properly take into account the substituent effects upon ^3J(H,H)-couplings in ethyl derivatives. In fact, in his equation, he included an additional $\sin(2\theta)$ term to improve the fitting. It was later utilized also by Altona [14,16] and in more recent studies [87,91–97] particularly devoted to carbohydrates.

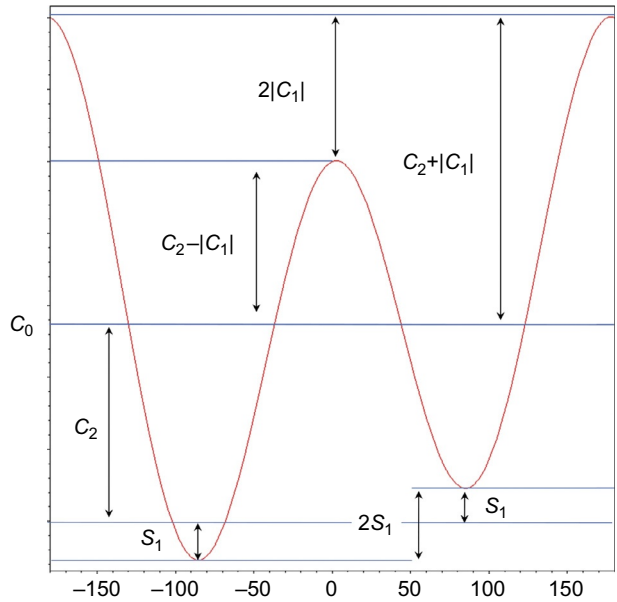

Figure 5.7 Physical interpretation of the Karplus coefficients of an equation of the form $J(\theta) = C_0 + C_1 \cos(\theta) + C_2 \cos(2\theta) + S_1 \sin(\theta)$. In this picture, the parameter C_1 is assumed to be negative and S_1 is positive.

In ordinary proteins, asymmetry is expected in coupling constants $^3J(H^{\alpha},H^{\beta})$, $^3J(N,H^{\beta})$, $^3J(C',H^{\beta})$, $^3J(H^{\alpha},C^{\gamma})$, $^3J(N,C^{\gamma})$, and $^3J(C',C^{\gamma})$, which are governed by the dihedral angle χ related to the amino acid side-chain torsion [83].

A more general representation that combines both high-order sine and cosine terms is given by the so-called generalized polar Karplus model of Schmidt [83]. The more general and extended functional dependence of the *J*-coupling of the form

$$J(\theta) = \sum_k C_k \cos(k\theta) + \sum_l S_l \sin(l\theta) \tag{5.9}$$

can be also expressed in a polar compact representation (provided that the same number of sine and cosine terms is considered) as

$$J(\theta) = \sum_k D_k \cos[k(\theta + \vartheta_k)], \tag{5.10}$$

where $C_k = D_k \cos \vartheta_k$, $S_k = D_k \sin \vartheta_k$, and $D_k = (C_k^2 + S_k^2)^{1/2}$ and $\vartheta_k = \text{atan}\left(\frac{S_k}{C_k}\right)$.

Considering terms up to $k = 2$, one obtains

$$J(\theta) = D_0 + D_1 \cos(\theta + \vartheta_1) + D_2 \cos[2(\theta + \vartheta_2)] \tag{5.11}$$

Now, the original Karplus relationship of Eq. (5.2) is recovered by setting $\vartheta_k = 0$ for all k, whereas the extended Eq. (5.8) is obtained by just setting $\vartheta_2 = 0$.

The functional dependence of Eq. (5.9) with up to $k = 3$ and $l = 2$ was recently used to fit DFT-computed vicinal J-couplings associated to the side-chain torsion of valine [98] and phenylalanine and tyrosine residues [99]. The authors found a relevant contribution from the S_2 term and rather unexpected positive C_1 coefficient. The latter has been interpreted in terms of hyperconjugative interactions [98,100,101].

Equation (5.10) also suggests that the torsion phase ϑ_k, which is given in a fix value in the context of self-consistent Karplus parameterizations discussed earlier (see Fig. 5.2), can also be seen and used as an extra parameter for the fitting.

Indeed, four-parameter equation of the form

$$J(\theta) = A \cos^2(\theta + \delta) + B \cos(\theta + \delta) + C \tag{5.12}$$

has been applied, among others, by Lindorff-Larsen [35], Case [102], and Chou [36] to parameterize the dependence of a number of vicinal ^3J-couplings associated to backbone and side-chain torsion angles in proteins from experimental and DFT data.

Further improvements of the quality of the fittings can be achieved by using extended Karplus models that can account for substituent effects. The well-known classical Haasnoot–Altona equation [12] for proton–proton vicinal J-couplings

$$J(\theta) = p_1 \cos^2\theta + p_2 \cos\theta + p_3 + \sum_{i=1}^{4} \Delta\chi_i \left[p_4 + p_5 \cos^2(\xi\theta + p_6|\Delta\chi_i|)\right] \tag{5.13}$$

uses six adjustable parameters $\{p_i\}$ and the substituent- and substituent-orientation-dependent parameters $\Delta\chi_i$ and ξ. The former accounts for electronegativity differences between the ith substituent and hydrogen. Improved parameterizations such as the Diez–Altona–Donders [17] also include sine terms to explicitly account for asymmetry effects. van

Gunsteren [31] recently applied this functional form to establish the dependence upon the side-chain torsional angle χ of $^3J(H^{\alpha},H^{\beta})$-couplings.

In the case of polypeptides, one could in principle improve the fit errors by making use of amino acid-type-dependent sets of Karplus coefficients. Schmidt [82] introduced a clever scheme in which fundamental Karplus parameters for a given *J*-coupling were combined with a dihedral angle-independent term (incremental coefficient) that accounts for the different amino acid topologies.

The functional form of the *J*-coupling model can be written as

$$J_{XY}(\theta) = C_0 + \Delta C_0 + C_1 \cos(\theta) + C_2 \cos(2\theta) \tag{5.14}$$

where $\Delta C_0 = \kappa \sum_i n_i \Delta C_0^{(i)}$ and $\kappa = \dfrac{(\gamma_X \gamma_Y)^{1/2}}{\gamma_H}$.

The $\Delta C_0^{(i)}$ incremental coefficients account for substituent effects (differences with respect to H atoms) in both the central and terminal sites, n_i being the number of counts each particular substitution i occurs. The prefactor κ is introduced in order to normalize the incremental effect on each *J*-coupling according to the magnitude of the gyromagnetic constants γ_X and γ_Y constants of the pair of nuclei involved.

Hence, the set of incremental coefficients $\Delta C_0^{(i)}$ is included in the fitting process. The authors used this formulation within a self-consistent fitting approach [81] to obtain very accurate amino acid-specific Karplus parameters for the six vicinal ^3J-couplings that probe the side-chain torsion angle χ by making use of six additional $\Delta C_0^{(i)}$ parameters. In a subsequent study, the results were further improved by introducing an additional sine term to account for asymmetry effects.

Further extensions of the Karplus equations have also been introduced to explore the dependencies of the *J*-couplings upon two dihedral angles simultaneously [73]. This strategy has been used to describe analytically the complex angular dependencies that often exhibit one- and two-bond *J*-couplings, for which the Karplus theory does not trivially applies. In some other cases, it has been observed that, even for vicinal ^3J-couplings, including explicit dependence of a second dihedral angle further improves the fitting. In the context of protein structure determination, the use of expressions depending upon the two backbone dihedral angles will potentially allow for a complete determination of the backbone conformation (i.e. secondary structure).

Edison *et al.* [103,104] fitted *ab initio* calculations of the Fermi contact term and experimental correlations of a number of ^1J-, ^2J-, and ^3J-couplings of a peptide model to a two-dimensional equation of the form

$$J(\phi,\psi)=\sum_{i=1}^{M}\sum_{j=1}^{N}\{\cos(i\phi)\cos(j\psi)+\cos(i\phi)\sin(j\psi) +\sin(i\phi)\cos(j\psi)+\sin(i\phi)\sin(j\psi)\} \tag{5.15}$$

(with appropriate coefficients for each independent term) in terms of the backbone ϕ and ψ angles. A second-order expansion with $M=N=2$ including 25 adjustable parameters produced a good fit.

Hennig *et al.* [105] used a first-order fit ($M=N=1$) utilizing nine adjustable parameters to establish the dependence of the $^3J(C^{\alpha},H^{N})$-coupling constants associated to the peptide-bond torsion ω_i with the adjacent ϕ_i and ψ_{i-1} backbone dihedral angles for structure determination.

However, the superiority of two-dimensional fits over the conventional one-dimensional ones sometimes leads to controversies. Wirmer [106] studied a set of $^2J(N_i,C^{\alpha}_{i-1})$-couplings from ubiquitin and staphylococcal nuclease and found significant correlation with backbone conformation. Using in this case a truncated two-dimensional Fourier series of the form

$$J(\theta_1,\theta_2)=C_0+\sum_{k=1}^{M}C_1^{(k)}\cos^k\theta_1+\sum_{k=1}^{N}C_2^{(k)}\cos^k\theta_2 \tag{5.16}$$

the fitting obtained with $M=N=2$ (five parameters) as a function of ϕ_{i-1} and ψ_{i-1} dihedrals was excellent. In the case of the $^1J(N_i,C^{\alpha}_i)$-coupling, however, the use of a two-dimensional fit was not statistically superior over a conventional one-dimensional Karplus function. Later on, Kozminski *et al.* [107] explored the same angular dependence for the $^2J(N_i,C^{\alpha}_{i-1})$-coupling using DFT calculations on a dipeptide model system with $M=2$ and $N=1$. Conversely, Puttonen *et al.* [108] found that a two-dimensional equation did not improve significantly over and a conventional Karplus fit of experimental $^2J(N_i,C^{\alpha}_{i-1})$-coupling values with the ψ_{i-1} dihedral angle. Most recently, Kazimierczuk *et al.* [109] were able to measure the full set of 72 $^2J(N_i,C^{\alpha}_{i-1})$-couplings on human ubiquitin and obtained a better two-dimensional fit to both ϕ_{i-1} and ψ_{i-1} dihedral angles.

Clearly, one of the reason of these kind of quandaries in establishing the dihedral dependences of the *J*-couplings is the lack of experimental data on significant parts of the conformational space. The backbone conformations typically populate the allowed regions of the Ramachandran space, and the

side-chain torsion is essentially restricted to the classical rotameric positions around $\chi = \pm 60°$ and $\chi = \pm 180°$. The data points of the representations of experimental *J*-couplings versus dihedral angle are typically clustered around the populated conformations. The lack of experimental sampling in significant parts of the ϕ, ψ, or χ space in the X-ray or NMR structures essentially makes several sets of Karplus parameters able to describe equally well the data. It is also difficult to determine whether a postulated dependence upon additional geometric parameters is significant or not. van Gunsteren [31] illustrated these problems most recently for the case of $^3J(H^{\alpha},H^{\beta})$-couplings, depending upon the side-chain torsional angle χ.

Thus, $^1J(N_i,C^{\alpha}_i)$, $^2J(N_i,C^{\alpha}_{i-1})$, and possibly other *J*-couplings could definitely be used as a secondary structure index, that is, to discriminate between most different conformations such as helical and beta-sheet, but one should abstain to use the corresponding Karplus fits to establish quantitative relations with dihedral angles. The use of these Karplus fits to estimate the *J*-coupling values from the averaging over an MD simulation trajectory that does sample the entire dihedral angle space is questionable [110].

In this sense, exploring the dependence of a given *J*-coupling over the entire range of values of the corresponding dihedral angle can be better achieved using *ab initio* calculations [24,47–76,80,87–104,107,111–123]. Whether or not the associated Karplus fit will improve over the empirical ones for structure determination critically depends on the ability of the computational model (i.e. combination of level of theory and basis sets and inclusion of solvent effects) to produce accurate *J*-coupling values.

An illustrative example is the recent study by Juranic [124] on the relationship of $^2J(N,C')$-couplings with the peptide-bond twist angle ω, typically assumed planar. The deviations of the peptide bond from planarity are very small, so that high-accuracy data are needed to establish significant relationships. Because such level of precision can hardly be achieved experimentally, the authors relied on DFT predictions for a capped tripeptide model system combined with the experimental data to derive a rather involved analytic relationship of the $^2J(N,C')$-coupling values with the planarity and relative orientation of the sequentially adjacent peptide-bond planes. It was noted that relatively large $^2J(N,C')$-couplings may be indicative of significant structural strain.

The state of the art of the quantum mechanical methods for the calculation of *J*-couplings has been most recently reviewed by Rusakov and Krivdin [125].

3.2. Nonanalytic Expressions

For those *J*-couplings not trivially considered within the Karplus theory such as ^{1}J- and ^{2}J-couplings, one is often left to statistical analysis aimed at looking for trends and correlations rather than to derive parameterizations. The recent vast studies of Schmidt on C^{α}-related ^{1}J-couplings [126] and ^{2}J-couplings [127] are noteworthy examples. He carried out an exhaustive statistical analysis of a set of 3999 measurements of ten different types of ^{2}J-couplings gathered from 148 NMR experiments on six proteins. The results indicated a strong correlation of the $^{2}J(C^{\alpha},N)$- and $^{2}J(H_N,C^{\alpha})$-couplings with both ϕ and ψ dihedral angles and a moderated but still significant correlation of the $^{2}J(H^{\alpha},C')$ and $^{2}J(C',H_N)$ ones [127]. In the case of the ^{1}J-couplings, the authors investigated all four one-bond couplings involving the C^{α} carbon of the polypeptide chain. A total of 3105 couplings constants from 150 NMR experiments from six proteins were subjected to extensive statistical analysis [126]. All four C^{α}-related ^{1}J-couplings were found equally sensitive to side-chain torsion angle (χ) and to backbone ϕ and ψ dihedral angles. Averaged values of some couplings were found to correlate to amino acid type rather than to structure, like the $^{1}J(C^{\alpha},C^{\beta})$-coupling, and some others did not exhibit significant variations, like the $^{1}J(C^{\alpha},C')$ ones. For both the ^{1}J- and the ^{2}J-couplings, the authors avoided any attempt to perform parameterizations of their dependence upon dihedral angles.

Theoretical electronic structure calculations, in particular the more affordable DFT methods, can also be applied to explore the dependence of *J*-couplings on backbone dihedral angles in an exhaustive fashion. Dannenberg *et al.* [123] used as a model an acetyl$(Ala)_3NH_2$ capped trialanine peptide to determine the dihedral angle dependence of up to 24 one-, two-, and three-bond *J*-coupling constants for the entire Ramachandran space of the central Ala residue at the B3LYP/D95** level of theory. Initially, full geometry optimizations for all degrees of freedom except dihedral ϕ and ψ of the central alanine residue were carried out for fixed 5° intervals each, in the full range of −180° to 180°, for a total number of 5184 optimized structures [128]. Then, the *J*-couplings involving essentially all pairs of atoms of the backbone and side chain were computed with varying intervals from 10° to 20° in both ϕ and ψ, for a total number of 483 single-point calculations. The study manifested significant deviations from Karplus-type models over a single dihedral angle, even for the widely used $^{3}J(H^{\alpha},H^{N})$-coupling (see Fig. 5.8).

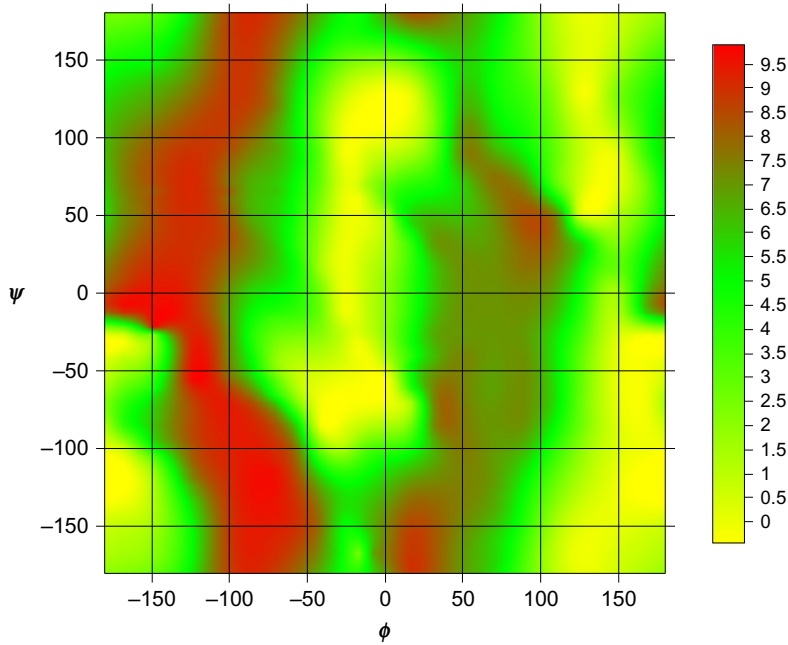

Figure 5.8 B3LYP/D95** $^3J(H^{\alpha},H^{N})$ couplings over the whole Ramachandran space of the central residue in Ac-Ala_3-NH_2 model. *Adapted from Ref. [123] with permission of the PCCP Owner societies.*

In fact, only the $^3J(C'_{i-1},C'_i)$-, $^3J(C'_{i-1},H^{\alpha})$-, and $^3J(C'_{i-1},C^{\beta})$-couplings exhibited the expected behaviour of a genuine Karplus dependence [123]. As could be anticipated, the ^1J- and ^2J-couplings depended on both backbone dihedral angles in a complex manner, as illustrated in Fig. 5.9 for the case of the $^1J(N,C')$-coupling constant.

Rather than fitting the *J*-couplings to analytic expressions of the dihedral angles, the authors provided with two-dimensional grids for each *J*-coupling from which the theoretical estimate for any pair of ϕ and ψ values could be obtained by simple interpolation (triangulation). Even though such strategy may not be so helpful for structure determination, the use of a numerical grid-based approach should be useful for accurate *J*-coupling predictions averaged over an MD trajectory or NMR ensemble structures, particularly in those cases where Karplus fits are not available or simply not appropriate.

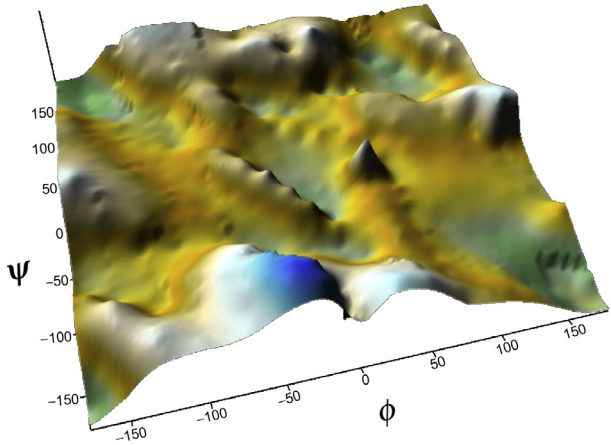

Figure 5.9 B3LYP/D95** ^{1}J(N,C′) couplings over the whole Ramachandran space of the central residue in Ac-Ala_3-NH_2 model. *Adapted from Ref. [123] with permission from the PCCP Owner societies.*

4. PARAMETERIZATIONS OF *J*-COUPLINGS UPON DIHEDRAL ANGLES IN PROTEINS

In this last section, we provide with an updated compilation of analytic Karplus and extended Karplus equations that describe the dependence of *J*-couplings (mostly vicinal ^{3}J ones) with the dihedral angles associated to the backbone and side-chain conformations of polypeptide chains.

Most of the data refer to the backbone's ϕ_i(C'_{i-1}–N–C^{α}–C'_i) angle (Tables 5.2–5.7) and side-chain χ(N–C^{α}–C^{β}–C^{γ}) torsion angles (Tables 5.8–5.13). These are best described by a number of vicinal ^{3}J-couplings.

In the case of the backbone's ψ_i(N_i–C^{α}–C′–N_{i+1}) dihedral angle, there are much fewer ^{3}J-couplings that can serve as experimental probes of it (see Table 5.14). Couplings involving oxygen atoms can hardly be determined with sufficient accuracy due to the quadruple moment and fast relaxation of ^{17}O nuclei. The ^{3}J(N,N)-coupling constants are very small and not too sensitive to neither ϕ nor ψ variations [123]. In addition, dihedral angle dependencies of two important ^{1}J- and ^{2}J-couplings typically used for protein structure determination are included in Tables 5.15 and 5.16.

Unless otherwise stated, we will discuss the *J*-coupling for the spin-1/2 isotopes such as ^{1}H, ^{13}C, and ^{15}N. As usual, *J*-couplings for alternative isotopes may be derived from the respective gyromagnetic ratios.

Table 5.2 Coefficients of Karplus-type equations for $J(\phi+\delta\phi)$ coupling constants

$\delta\phi=0^\circ$	A/C_0	B/C_1	C/C_2	Additional parameters	Fitting method	Source (n)	Eq. type (see text)	References
$^3J(C'_{i-1},C'_i)$	2.71	−0.91	0.21	−2.56	Rigid, DFT	Ace-Ala-NH_2	(5.12)	[102]
$^3J(C'_{i-1},C'_i)$	1.36	−0.93	0.60	n/a	Rigid[a], NMR [129,130]	Ubiquitin (57)	(5.3)	[130]
$^3J(C'_{i-1},C'_i)$	1.51 ± 0.86	-1.09 ± 1.11	0.52 ± 0.39	n/a	Self-consistent	Flavodoxin (745)	(5.2)	[79]

The $\delta\phi$ angle shifts relate the torsion angle between the particular pairs of spins to ϕ. See text for the particular Karplus equation type used. Fitting method applied, data source, and the number of J-couplings used in the fitting (in parenthesis) are also given.
[a]Best performing Karplus fit. Alternative formulations are available in the original publication.

Table 5.3 Coefficients of Karplus-type equations for $J(\phi+\delta\phi)$ coupling constants

$\delta\phi=-120^\circ$	A/C_0	B/C_1	C/C_2	Additional parameters	Fitting method	Source (n)	Eq. type (see text)	References
$^3J(C'_{i-1},C^\beta)$	1.86	−1.20	0.27	2.45	Rigid, DFT	Ace-Ala-NH_2	(5.12)	[102]
$^3J(C'_{i-1},C^\beta)$	1.74	−0.57	0.25	n/a	Rigid[a], NMR [129,130]	Ubiquitin (57)	(5.3)	[130]
$^3J(C'_{i-1},C^\beta)$	2.72 ± 0.80	-0.31 ± 0.52	0.39 ± 0.37	n/a	Self-consistent	Flavodoxin (745)	(5.2)	[79]

The $\delta\phi$ angle shifts relate the torsion angle between the particular pairs of spins to ϕ. See text for the particular Karplus equation type used. Fitting method applied, data source, and the number of J-couplings used in the fitting (in parenthesis) are also given.
[a]Best performing Karplus fit. Alternative formulations are available in the original publication.

Table 5.4 Coefficients of Karplus-type equations for $J(\phi+\delta\phi)$ coupling constants

$\delta\phi = 120^\circ$	A/C_0	B/C_1	C/C_2	Additional parameters	Fitting method	Source (n)	Eq. type (see text)	References
$^3J(C'_{i-1},H^\alpha)$	4.41 ± 0.06	-2.14 ± 0.03	0.77 ± 0.05	n/a	Ensemble, DER [32] (128)	Ubiquitin (65)	(5.3)	[35]
$^3J(C'_{i-1},H^\alpha)$	4.77	−1.85	0.49	−1.49	Rigid, DFT	Ace-Ala-NH_2	(5.12)	[102]
$^3J(C'_{i-1},H^\alpha)$	3.72	−2.18	1.28	n/a	Rigid[a], NMR [129,130]	Ubiquitin (57)	(5.3)	[130]
$^3J(C'_{i-1},H^\alpha)$	3.76 ± 1.05	-1.63 ± 0.56	0.89 ± 0.60	n/a	Self-consistent	Flavodoxin (745)	(5.2)	[79]

The $\delta\phi$ angle shifts relate the torsion angle between the particular pairs of spins to ϕ. See text for the particular Karplus equation type used. Fitting method applied, data source, and the number of J-couplings used in the fitting (in parenthesis) are also given.
[a]Best performing Karplus fit. Alternative formulations are available in the original publication.

Table 5.5 Coefficients of Karplus-type equations for $J(\phi+\delta\phi)$ coupling constants

$\delta\phi = 60^\circ$	A/C_0	B/C_1	C/C_2	Additional parameters	Fitting method	Source (n)	Eq. type (see text)	References
$^3J(H^N,C^\beta)$	5.5 ± 0.1	-1.30 ± 0.04	-0.16 ± 0.02	n/a	Ensemble, DER [32] (128)	Ubiquitin (60)	(5.3)	[35]
$^3J(H^N,C^\beta)$	3.71	−0.59	0.08	n/a	Ensemble[a] (160) [33]	GB3 (49)	(5.3)	[24]
$^3J(H^N,C^\beta)$	4.58	−0.36	−0.31	−1.82	Rigid, DFT	Ace-Ala-NH_2	(5.12)	[102]
$^3J(H^N,C^\beta)$	3.06	−0.74	0.13	n/a	Rigid[a], NMR [129,130]	Ubiquitin (57)	(5.3)	[130]
$^3J(H^N,C^\beta)$	2.90 ± 0.80	-0.56 ± 0.52	0.18 ± 0.37	n/a	Self-consistent	Flavodoxin (745)	(5.2)	[79]

The $\delta\phi$ angle shifts relate the torsion angle between the particular pairs of spins to ϕ. See text for the particular Karplus equation type used. Fitting method applied, data source, and the number of J-couplings used in the fitting (in parenthesis) are also given.
[a]Best performing Karplus fit. Alternative formulations are available in the original publication.

Table 5.6 Coefficients of Karplus-type equations for $J(\phi+\delta\phi)$ coupling constants

$\delta\phi=+180^\circ$	A/C_0	B/C_1	C/C_2	Additional parameters	Fitting method	Source (n)	Eq. type (see text)	References
$^3J(H^N,C'_i)$	3.4 ± 0.1	-0.75 ± 0.08	-0.08 ± 0.03	n/a	Ensemble, DER [32] (128)	Ubiquitin (61)	(5.3)	[35]
$^3J(H^N,C'_i)$	4.36	−1.08	−0.01	n/a	Ensemble[a] (160) [33]	GB3 (49)	(5.3)	[24]
$^3J(H^N,C'_i)$	5.34	−1.46	−0.29	−7.51	Rigid, DFT	Ace-Ala-NH_2	(5.12)	[102]
$^3J(H^N,C'_i)$	4.29	−1.01	0.00	n/a	Rigid[a], NMR [129,130]	Ubiquitin (57)	(5.3)	[130]
$^3J(H^N,C'_i)$	4.41 ± 0.81	-1.36 ± 1.03	0.24 ± 0.37	n/a	Self-consistent	Flavodoxin (745)	(5.2)	[79]

The $\delta\phi$ angle shifts relate the torsion angle between the particular pairs of spins to ϕ. See text for the particular Karplus equation type used. Fitting method applied, data source, and the number of J-couplings used in the fitting (in parenthesis) are also given.
[a]Best performing Karplus fit. Alternative formulations are available in the original publication.

Table 5.7 Coefficients of Karplus-type equations for $J(\phi+\delta\phi)$ coupling constants

$\delta\phi=-60^\circ$	A/C_0	B/C_1	C/C_2	Additional parameters	Fitting method	Source (n)	Eq. type (see text)	References
$^3J(H^N,H^\alpha)$	8.40	−1.36	0.33	n/a	Ensemble[a] (160) [33]	GB3 (49)	(5.3)	[24]
$^3J(H^N,H^\alpha)$	8.33 ± 0.06	-1.69 ± 0.03	0.44 ± 0.05	n/a	Ensemble, DER [32] (128)	Ubiquitin (63)	(5.3)	[35]
$^3J(H^N,H^\alpha)$	9.14	−2.28	−0.29	−4.51	Rigid, DFT	Ace-Ala-NH_2	(5.12)	[102]
$^3J(H^N,H^\alpha)$	7.09	1.42	1.55	n/a	Rigid[a], NMR [129,130]	Ubiquitin (57)	(5.3)	[130]
$^3J(H^N,H^\alpha)$	7.90 ± 1.02	-1.05 ± 0.54	0.65 ± 0.58	n/a	Self-consistent	Flavodoxin (745)	(5.2)	[79]

The $\delta\phi$ angle shifts relate the torsion angle between the particular pairs of spins to ϕ. See text for the particular Karplus equation type used. Fitting method applied, data source, and the number of J-couplings used in the fitting (in parenthesis) are also given.
^3J-couplings as a function of the $\chi(N–C^\alpha–C^\beta–C^\gamma)$ side-chain torsion angle.
[a]Best performing Karplus fit. Alternative formulations are available in the original publication.

Table 5.8 Coefficients of Karplus-type equations for $J(\chi+\delta\chi)$ coupling constants

$\delta\chi=-120^\circ$	A/C_0	B/C_1	C/C_2	Additional parameters	Fitting method	Source (*n*)	Eq. type (see text)	References
$^3J(C',C^\gamma)$	1.70	−0.70	1.72	0.14 (C_3) 0.11 (S_1) −0.15 (S_2)	Rigid, DFT	Ace-Val-NME	(5.9)	[98]
$^3J(C',C^\gamma)$	1.69[a]	−1.11	1.11	0.10 (S_1)	Self-consistent	Flavodoxin (763)	(5.14)	[30]
$^3J(C',C^\gamma)$	1.70[a]	−0.87	1.15	n/a	Self-consistent	Flavodoxin (763)	(5.2)	[82]
$^3J(C',C^\gamma)$[b]	3.42	−0.59	0.17	5	Ensemble, NMR [36]	Ubiquitin, GB3, HIV-protease (51)	(5.12)	[36]
$^3J(C',C^\gamma)$[c]	2.76	−0.67	0.19	17	Ensemble, NMR [36]	Ubiquitin, GB3, HIV-protease (51)	(5.12)	[36]

The $\delta\chi$ angle shifts relate the torsion angle between the particular pairs of spins to χ. See text for the particular Karplus equation type used. Fitting method applied, data source, and the number of *J*-couplings used in the fitting (in parenthesis) are also given.
[a]Consensus values. Specific C_0 parameters for different amino acid types are available in the original publication.
[b]From Val and Ile residues. See original publication for the definition of C^γ.
[c]From Thr residues. See original publication for the definition of C^γ.

Table 5.9 Coefficients of Karplus-type equations for $J(\chi+\delta\chi)$ coupling constants

$\delta\chi=0^\circ$	A/C_0	B/C_1	C/C_2	Additional parameters	Fitting method	Source (n)	Eq. type (see text)	References
$^3J(C',H^\beta)$	3.77	−0.97	3.63	−0.20 (C_3) −0.07 (S_1) −0.10 (S_2)	Rigid, DFT	Ace-Val-NME	(5.9)	[98]
$^3J(C',H^\beta)$	3.24[a]	−1.99	2.48	−0.59 (S_1)	Self-consistent	Flavodoxin (763)	(5.14)	[30]
$^3J(C',H^\beta)$	3.32[a]	−1.58	2.01	n/a	Self-consistent	Flavodoxin (763)	(5.2)	[82]

The $\delta\chi$ angle shifts relate the torsion angle between the particular pairs of spins to χ. See text for the particular Karplus equation type used. Fitting method applied, data source, and the number of J-couplings used in the fitting (in parenthesis) are also given.

[a]Consensus values. Specific C_0 parameters for different amino acid types are available in the original publication.

Table 5.10 Coefficients of Karplus-type equations for $J(\chi+\delta\chi)$ coupling constants

$\delta\chi=120^\circ$	A/C_0	B/C_1	C/C_2	Additional parameters	Fitting method	Source (n)	Eq. type (see text)	References
$^3J(H^\alpha,C^\gamma)$	4.03	1.10	3.66	0.02 (C_3) 0.22 (S_1) 0.70 (S_2)	Rigid, DFT	Ace-Val-NME	(5.9)	[98]
$^3J(H^\alpha,C^\gamma)$	3.41[a]	−1.58	2.46	0.10 (S_1)	Self-consistent	Flavodoxin (763)	(5.14)	[30]
$^3J(H^\alpha,C^\gamma)$	3.46[a]	−0.96	2.67	n/a	Self-consistent	Flavodoxin (763)	(5.2)	[82]

The $\delta\chi$ angle shifts relate the torsion angle between the particular pairs of spins to χ. See text for the particular Karplus equation type used. Fitting method applied, data source, and the number of J-couplings used in the fitting (in parenthesis) are also given.

[a]Consensus values. Specific C_0 parameters for different amino acid types are available in the original publication.

Table 5.11 Coefficients of Karplus-type equations for $J(\chi+\delta\chi)$ coupling constants

$\delta\chi=0^\circ$	A/C_0	B/C_1	C/C_2	Additional parameters	Fitting method	Source (n)	Eq. type (see text)	References
$^3J(H^\alpha,H^\beta)$	6.61	−1.07	3.36	n/a	Ensemble, NMR (16)[b]	Plastocyanin (108)	(5.3)	[31]
$^3J(H^\alpha,H^\beta)$	5.87	−1.59	3.50	n/a	Ensemble, X-ray (2)[b]	HEWL (100)	(5.3)	[31]
$^3J(H^\alpha,H^\beta)$	6.41	0.89	5.58	−0.18 (C_3) −0.10 (S_1) 1.36 (S_2)	Rigid, DFT	Ace-Val-NME	(5.9)	[98]
$^3J(H^\alpha,H^\beta)$	5.86[a]	−1.86	3.81	−0.37	Self-consistent	Flavodoxin (763)	(5.14)	[30]
$^3J(H^\alpha,H^\beta)$	5.83[a]	−1.37	3.61	n/a	Self-consistent	Flavodoxin (763)	(5.2)	[82]
$^3J(H^\alpha,H^\beta)$	5.34	−0.65	3.70	n/a	X-ray[b]	FKBP (94)	(5.3)	[31]

The $\delta\chi$ angle shifts relate the torsion angle between the particular pairs of spins to χ. See text for the particular Karplus equation type used. Fitting method applied, data source, and the number of J-couplings used in the fitting (in parenthesis) are also given.

[a]Consensus values. Specific C_0 parameters for different amino acid types are available in the original publication.

[b]Best performing Karplus fit. Alternative formulations are available in the original publication.

Table 5.12 Coefficients of Karplus-type equations for $J(\chi+\delta\chi)$ coupling constants

$\delta\chi=0°$	A/C_0	B/C_1	C/C_2	Additional parameters	Fitting method	Source (n)	Eq. type (see text)	References
$^3J(\mathrm{N,C}^\gamma)$	2.8 ± 0.2	0.4 ± 0.1	-0.4 ± 0.1	3 ± 0.1	Ensemble, DER [32] (128)	Ubiquitin (14) TNfne (15)	(5.12)	[35]
$^3J(\mathrm{N,C}^\gamma)$	0.83	0.23	0.87	0.14 (C_3) 0.07 (S_1) -0.01 (S_2)	Rigid, DFT	Ace-Val-NME	(5.9)	[98]
$^3J(\mathrm{N,C}^\gamma)$	3.5	0.40	-0.2	n/a	Rigid, X-ray	Parvalbumin (6), Calmodulin (12), IFAPB (2)	(5.3)	[131]
$^3J(\mathrm{N,C}^\gamma)$	1.05[a]	-0.55	0.68	0.02	Self-consistent	Flavodoxin (763)	(5.14)	[30]
$^3J(\mathrm{N,C}^\gamma)$	1.02[a]	-0.49	0.65	n/a	Self-consistent	Flavodoxin (763)	(5.2)	[82]
$^3J(\mathrm{N,C}^\gamma)$[b]	2.64	0.26	-0.22	6	Ensemble, NMR [36]	Ubiquitin, GB3, HIV-protease (51)	(5.12)	[36]
$^3J(\mathrm{N,C}^\gamma)$[c]	2.01	-0.21	0.12	7	Ensemble, NMR [36]	Ubiquitin, GB3, HIV-protease (51)	(5.12)	[36]

The $\delta\chi$ angle shifts relate the torsion angle between the particular pairs of spins to χ. See text for the particular Karplus equation type used. Fitting method applied, data source, and the number of J-couplings used in the fitting (in parenthesis) are also given.
[a]Consensus values. Specific C_0 parameters for different amino acid types are available in the original publication.
[b]From Val and Ile residues. See original publication for the definition of C^γ.
[c]From Thr residues. See original publication for the definition of C^γ.

Table 5.13 Coefficients of Karplus-type equations for $J(\chi+\delta\chi)$ coupling constants

$\delta\chi=-120°$	A/C_0	B/C_1	C/C_2	Additional parameters	Fitting method	Source (n)	Eq. type (see text)	References
$^3J(N,H^\beta)$	1.86	0.41	1.85	0.11 (C_3) −0.11 (S_1) 0.08 (S_2)	Rigid, DFT	Ace-Val-NME	(5.9)	[98]
$^3J(N,H^\beta)$	2.15[a]	−0.93	1.26	0.17	Self-consistent	Flavodoxin (763)	(5.14)	[30]
$^3J(N,H^\beta)$	2.22[a]	−0.75	1.15	n/a	Self-consistent	Flavodoxin (763)	(5.2)	[82]

The $\delta\chi$ angle shifts relate the torsion angle between the particular pairs of spins to χ. See text for the particular Karplus equation type used. Fitting method applied, data source, and the number of J-couplings used in the fitting (in parenthesis) are also given.
^3J-couplings as a function of the $\psi(N_i–C^\alpha–C'–N_{i+1})$ backbone torsion angle.
[a]Consensus values. Specific C_0 parameters for different amino acid types are available in the original publication.

Table 5.14 Coefficients of Karplus-type equations for $^3J(\psi)$ and/or $^3J(\psi,\phi)$ coupling constants

	A/C_0	B/C_1	C/C_2	Additional parameters	Fitting method	Source (n)	Eq. type (see text)	References
$^3J(H^{\alpha},N_{i+1})$[a]	5.58	−1.06	−0.30		Rigid, DFT	Ace-Ala-NH_2	(5.3)	[102]
$^3J(H^{\alpha},N_{i+1})$[a,b]	−0.88	−0.61	−0.27		Rigid, X-ray [132]	Ubiquitin (67)	(5.3)	[133]
$^3J(C^{\alpha},H^{N})$	0.5390	–	–	−0.2280[c] −0.2026 0.0680 0.0802 0.0664 0.1209 −0.0798 −0.1367	Rigid, X-ray	Ubiquitin (67)	(5.15)	[105]

See text for the particular Karplus equation type used. Fitting method applied, data source, and the number of J-couplings used in the fitting (in parenthesis) are also given.
[a]See the original publication for additional constant-phase angles.
[b]Fit to the value of the J-coupling including negative sign.
[c]Coefficients of a two-dimensional Fourier series expansion including ϕ angle. See original publication for further details.

Table 5.15 Coefficients of Karplus-type equations for $^2J(\psi)$ and/or $^2J(\psi,\phi)$ coupling constants

	A/C_0	B/C_1	C/C_2	Additional parameters	Fitting method	Source (n)	Eq. type (see text)	References
$^2J(N_i,C^{\alpha}_{i-1})$	7.738	−1.557	−0.2047	n/a	Rigid, NMR	Ubiquitin (68)	(5.3)	[108]
$^2J(N_i,C^{\alpha}_{i-1})$[a,b]	−7.21	+1.41	−0.42	−0.47[c]	Rigid, X-ray	Ubiquitin (72)	(5.16)	[74]
$^2J(N_i,C^{\alpha}_{i-1})$[a,b]	−10.1982	−1.2395	−0.4346	−0.8664[c]	Rigid, DFT	Ace-Ala-NME	(5.16)	[107]
$^2J(N_i,C^{\alpha}_{i-1})$	7.8509	−1.517	−0.6616	n/a	Rigid, NMR	GB1 (55)	(5.3)	[134]
$^2J(N_i,C^{\alpha}_{i-1})$	7.8163	−1.3892	−0.3709	−0.1717[c] −0.6408[d]	Rigid, X-ray	Ubiquitin, staphylococcal nuclease (122)	(5.16)	[106]

See text for the particular Karplus equation type used. Fitting method applied, data source, and the number of J-couplings used in the fitting (in parenthesis) are also given.
[a]Fit to the value of the J-coupling including negative sign.
[b]See the original publication for additional constant-phase angles.
[c]C_1 coefficient for a cos ϕ dihedral angle additional term.
[d]C_2 coefficient for a $\cos^2\phi$ dihedral angle additional term.

Table 5.16 Coefficients of Karplus-type equations for $^1J(\psi)$ and/or $^1J(\psi,\phi)$ coupling constants

	A/C_0	B/C_1	C/C_2	Additional parameters	Fitting method	Source (n)	Eq. type (see text)	References
$^1J(N_i,C^\alpha_i)$	8.6453	−1.2129	2.8484	n/a	Rigid, NMR	GB1 (55)	(5.3)	[134]
$^1J(N_i,C^\alpha_i)$	9.2297	−1.0515	1.9386	n/a	Rigid, NMR	Ubiquitin (68)	(5.3)	[108]
$^1J(N_i,C^\alpha_i)$	9.5098	−0.9799	1.7040	n/a	Rigid, X-ray	Ubiquitin, staphylococcal nuclease (122)	(5.3)	[106]
$^1J(N_i,C^\alpha_i)$	10.176	−0.987	1.080	n/a	Rigid, X-ray	Ubiquitin (72)	(5.2)	[74]

See text for the particular Karplus equation type used. Fitting method applied, data source, and the number of J-couplings used in the fitting (in parenthesis) are also given.

ACKNOWLEDGEMENTS

Financial help has been furnished by the Spanish MICINN Project No. CTQ2011-23441/BQU. Financial support from MICINN and the FEDER fund (European Fund for Regional Development) was also provided by grant UNGI08-4E-003. Financial support from the Generalitat de Catalunya (SGR528 and Xarxa de Referencia en Quimica Teorica i Computacional) is also acknowledged. Profs. N. Juranic and J. J. Dannenberg are thanked for stimulating discussions. Dr. Anna Diaz-Cirac kindly helped in the preparation of the graphical support.

REFERENCES

[1] C. Peter, X. Daura, W.F. van Gunsteren, Peptides of aminoxy acids: a molecular dynamics simulation study of conformational equilibria under various conditions, J. Am. Chem. Soc. 122 (2000) 7461–7466.
[2] Z. Gattin, J. Zaugg, W.F. van Gunsteren, Structure determination of a flexible cyclic peptide based on NMR and MD simulation ^{3}J-coupling, Chem. Phys. Chem. 11 (2010) 830–835.
[3] M. Karplus, Contact electron-spin coupling of nuclear magnetic moments, J. Chem. Phys. 30 (1959) 11.
[4] M. Karplus, Vicinal proton coupling in nuclear magnetic resonance, J. Am. Chem. Soc. 85 (1963) 2870–2871.
[5] M. Barfield, M. Karplus, Valence-bond bond-order formulation for contact nuclear spin-spin coupling, J. Am. Chem. Soc. 91 (1969) 1.
[6] R.J. Abraham, G. Gatti, Rotational isomerism. Part VII. Effect of substituents on vicinal coupling constants in $XCH_2 \cdot CH_2Y$ fragments, J. Chem. Soc. B (1969) 961, http://pubs.rsc.org/en/content/articlelanding/1969/j2/j29690000961#!divAbstract.
[7] P.L. Durette, D. Horton, Conformational studies on pyranoid sugar derivatives by NMR spectroscopy. Correlations of observed proton–proton coupling constants with the generalized Karplus equation, Org. Magn. Reson. 3 (1971) 417.
[8] K.G.R. Pachler, Extended Hückel theory MO calculations of proton–proton coupling constants-II. The effect of substituents on vicinal couplings in monosubstituted ethanes, Tetrahedron 27 (1971) 187–199.
[9] L. Phillips, V. Wray, The structural dependence of the inductive effect. Part VI. The calculation of vicinal proton–proton spin–spin coupling constants in substituted ethanes, J. Chem. Soc. Perkin Trans. 11 (1972) 536.
[10] C.A.G. Haasnoot, F.A.A.M. de Leeuw, H.P.M. de Leeuw, C. Altona, Interpretation of vicinal proton–proton coupling constants by a generalized Karplus relation. Conformational analysis of the exocyclic C-4'–C-5' bond in nucleosides and nucleotides, Recueil J. R. Netherlands Chem. Soc. 98 (1979) 576–577.
[11] C.A.G. Haasnoot, F.A.A.M. de Leeuw, C. Altona, The relationship between proton–proton NMR coupling constants and substituent electronegativities-I. An empirical generalization of the Karplus equation, Tetrahedron 36 (1980) 2783.
[12] C.A.G. Haasnoot, F.A.A.M. de Leeuw, H.P.M. de Leeuw, C. Altona, The relationship between proton–proton NMR coupling constants and substituent electronegativities. II-Conformational analysis of the sugar ring in nucleosides and nucleotides in solution using a generalized Karplus equation, Org. Magn. Reson. 15 (1981) 43–52.
[13] C.A.G. Haasnoot, F.A.A.M. de Leeuw, C. Altona, Relationship between proton–proton NMR coupling constants and substituent electronegativities. III. Conformational analysis of proline rings in solution using a generalized Karplus equation, Biopolymers 20 (1981) 1211–1245.

[14] L.A. Donders, F.A.A.M. de Leeuw, C. Altona, Relationship between proton–proton NMR coupling constants and substituent electronegativities. IV. An extended Karplus equation accounting for interaction between substituents and its application to coupling constant data calculated by the extended Hückel method, Magn. Reson. Chem. 27 (1989) 556–563.
[15] C. Altona, J.H. Ippel, A.J.A. Westra Hoekzema, C. Erkelens, M. Groesbeek, L.A. Donders, Relationship between proton–proton NMR coupling constants and substituent electronegativities. V. Empirical substituent constants derived from ethanes and propanes, Magn. Reson. Chem. 27 (1989) 564–576.
[16] C. Altona, R. Francke, R. de Haan, J.H. Ippel, G.J. Daalmans, A.J.A. Westra Hoekzema, J. van Wijk, Empirical group electronegativities for vicinal NMR proton–proton couplings along a C–C bond: solvent effects and reparameterization of the Haasnoot equation, Magn. Reson. Chem. 32 (1994) 670–678.
[17] E. Diez, J. San-Fabian, J. Guilleme, C. Altona, L.A. Donders, Vicinal proton–proton coupling constants. I. Formulation of an equation including interactions between substituents, Mol. Phys. 68 (1989) 49.
[18] C. Altona, D.M. Grant, R. Morris (Eds.), Vicinal Coupling Constants and Conformation of Biomolecules, Wiley, New York, 1996, pp. 4909–4923.
[19] J. Mullay, Calculation of group electronegativity, J. Am. Chem. Soc. 107 (1985) 7271.
[20] W.J. Colucci, S.J. Jungk, R.D. Gandour, An equation utilizing empirically derived substituent constants for the prediction of vicinal coupling constants in substituted ethanes, Magn. Reson. Chem. 23 (1985) 335.
[21] W.J. Colucci, R.D. Gandour, E.A. Mooberry, Conformational analysis of charged flexible molecules in water by application of a new Karplus equation combined with MM2 computations: conformations of carnitine and acetylcarnitine, J. Am. Chem. Soc. 108 (1986) 7141.
[22] K. Imai, E. Osawa, An empirical extension of the Karplus equation, Magn. Reson. Chem. 28 (1990) 668.
[23] E. Osawa, T. Ouchi, N. Saito, M. Yamato, O.S. Lee, M.-K. Seo, Critical evaluation of an empirically modified Karplus equation, Magn. Reson. Chem. 30 (1992) 1104.
[24] B. Vogeli, J. Ying, A. Grishaev, A. Bax, Limits on variations in protein backbone dynamics from precise measurements of scalar couplings, J. Am. Chem. Soc. 129 (2007) 9377–9385.
[25] J.P. Derrick, D.B. Wigley, The third IgG-binding domain from streptococcal protein G: an analysis by X-ray crystallography of the structure alone and in a complex with Fab, J. Mol. Biol. 243 (1994) 906–918.
[26] T.S. Ulmer, B.E. Ramirez, F. Delaglio, A. Bax, Evaluation of backbone proton positions and dynamics in a small protein by liquid crystal NMR spectroscopy, J. Am. Chem. Soc. 125 (2003) 9179–9191.
[27] J.M. Schmidt, Conformational equilibria in polypeptides. II. Dihedral-angle distribution in antamanide based on three-bond coupling information, J. Magn. Reson. 124 (1997) 310–322.
[28] R. Brüschweiler, D.A. Case, Adding harmonic motion to the Karplus relation for spin-spin coupling, J. Am. Chem. Soc. 116 (1994) 11199–11200.
[29] H. Kessler, C. Griesinger, K. Wagner, Peptide conformations. 42. Conformation of side chains in peptides using heteronuclear coupling constants obtained by two-dimensional NMR spectroscopy, J. Am. Chem. Soc. 109 (1987) 6927–6933.
[30] J.M. Schmidt, Transforming between discrete and continuous angle distribution models: application to protein $\xi 1$ torsions, J. Biomol. NMR 54 (2012) 97–114.
[31] D. Steiner, J.R. Allison, A.P. Eichenberger, W.F. van Gunsteren, On the calculation of $3J\alpha\beta$-coupling constants for side chains in proteins, J. Biomol. NMR 53 (2012) 223–246.

[32] K. Lindorff-Larsen, R.B. Best, M.A. DePristo, C.M. Dobson, M. Vendruscolo, Simultaneous determination of protein structure and dynamics, Nature 433 (2005) 128–132.
[33] G.M. Clore, C.D. Schwieters, Concordance of residual dipolar couplings, backbone order parameters and crystallographic B-factors for a small a/ß protein: a unified picture of high probability, fast atomic motions in proteins, J. Mol. Biol. 355 (2006) 879–886.
[34] G.M. Clore, C.D. Schwieters, How much backbone motion in ubiquitin is required to account for dipolar coupling data measured in multiple alignment media as assessed by independent cross-validation? J. Am. Chem. Soc. 126 (2004) 2923–2938.
[35] K. Lindorff-Larsen, R.B. Best, M. Vendruscolo, Interpreting dynamically-averaged scalar couplings in proteins, J. Biomol. NMR 32 (2005) 273–280.
[36] J.J. Chou, D.A. Case, A. Bax, Insights into the mobility of methyl-bearing side chains in proteins from $^{3}J_{CC}$ and $^{3}J_{CN}$ couplings, J. Am. Chem. Soc. 125 (2003) 8959–8966.
[37] V. Sychrovsky, J. Grafenstein, D. Cremer, Nuclear magnetic resonance spin–spin coupling constants from coupled perturbed density functional theory, J. Chem. Phys. 113 (2000) 3530.
[38] T. Helgaker, M. Watson, N.C. Handy, Analytical calculation of nuclear magnetic resonance indirect spin–spin coupling constants at the generalized gradient approximation and hybrid levels of density-functional theory, J. Chem. Phys. 113 (2000) 9402.
[39] V. Barone, J.E. Peralta, R.H. Contreras, J.P. Snyder, DFT calculation of NMR J_{FF} spin-spin coupling constants in fluorinated pyridines, J. Chem. Phys. 106 (2002) 5607.
[40] S.A. Joyce, J.R. Yates, C.J. Pickard, F. Mauri, A first principles theory of nuclear magnetic resonance J-coupling in solid-state systems, J. Chem. Phys. 127 (2007) 204107.
[41] A. Møgelhøj, K. Aidas, K.V. Mikkelsen, S.P.A. Sauer, J. Kongsted, Prediction of spin-spin coupling constants in solution based on combined density functional theory/molecular mechanics, J. Chem. Phys. 130 (2009) 134508.
[42] N.F. Ramsey, Electron coupled interactions between nuclear spins in molecules, Phys. Rev. 91 (1953) 303.
[43] T. Helgaker, M. Jaszunski, K. Ruud, A. Gorska, Basis-set dependence of nuclear spin-spin coupling constants, Theor. Chem. Acc. 99 (1998) 175.
[44] P.F. Provasi, G.A. Aucar, S.P.A. Sauer, The effect of lone pairs and electronegativity on the indirect nuclear spin–spin coupling constants in CHX (X = CH, NH, O, S): ab initio calculations using optimized contracted basis sets, J. Chem. Phys. 115 (2001) 1324.
[45] J.E. Peralta, G.E. Scuseria, J.R. Cheeseman, M. Frisch, Basis set dependence of NMR spin–spin couplings in density functional theory calculations: first row and hydrogen atoms, J. Chem. Phys. Lett. 375 (2003) 452.
[46] J. Jokisaari, J. Autschbach, 13C–77Se and 77Se–77Se spin–spin coupling tensors in carbon diselenide: NMR experiments and ZORA DFT calculations, J. Phys. Chem. Chem. Phys. 5 (2003) 4551.
[47] P. Salvador, J.J. Dannenberg, Dependence upon basis sets of trans hydrogen-bond 13C-15N 3-bond and other scalar J-couplings in amide dimers used as peptide models. A density functional theory study, J. Phys. Chem. B 108 (2004) 15370.
[48] M. Sanchez, P.F. Provasi, G.A. Aucar, S.P.A. Sauer, On the usage of locally dense basis sets in the calculation of NMR indirect nuclear spin–spin coupling constants: vicinal fluorine–fluorine couplings, Adv. Quant. Chem. 48 (2005) 161.
[49] Y.Y. Rusakov, L.B. Krivdin, E.Y. Schmidt, A.I. Mikhaleva, B.A. Trofimov, Nonempirical calculations of NMR indirect spin–spin coupling constants. Part 15: pyrrolylpyridines, Magn. Reson. Chem. 44 (2006) 692.
[50] W. Deng, J.R. Cheeseman, M.J. Frisch, Calculation of nuclear spin-spin coupling constants of molecules with first and second row atoms in study of basis set dependence, J. Chem. Theor. Comput. 2 (2006) 1028.
[51] F. Jensen, The basis set convergence of spin-spin coupling constants calculated by density functional methods, J. Chem. Theor. Comput. 2 (2006) 1360.

[52] P. Manninen, J. Vaara, Systematic Gaussian basis set limit using completeness-optimized primitive sets. A case for magnetic properties, J. Comput. Chem. 27 (2006) 434.
[53] F. Jensen, Basis set convergence of nuclear magnetic shielding constants calculated by density functional methods, J. Chem. Theor. Comput. 4 (2008) 719.
[54] T. Kupka, From correlation-consistent to polarization-consistent basis sets estimation of NMR spin–spin coupling constant in the B3LYP Kohn–Sham basis set limit, Chem. Phys. Lett. 461 (2008) 33.
[55] F. Jensen, The optimum contraction of basis sets for calculating spin–spin coupling constants, Theor. Chem. Acc. 126 (2010) 371–382.
[56] M.-L. Jimeno, I. Alkorta, J. Elguero, J.E. Del Bene, Computed coupling constants in $X(CH_3)_nH_{(4-n)}$ moieties where X = ^{13}C and ^{15}N+, and n = 0–4: comparisons with experimental data, Magn. Reson. Chem. 44 (2006) 698.
[57] J.E. Del Bene, I. Alkorta, I.J. Elguero, A systematic comparison of second-order polarization propagator approximation (SOPPA) and equation-of-motion coupled cluster singles and doubles (EOM − CCSD) spin − spin coupling constants for selected singly bonded molecules, and the hydrides NH_3, H_2O, and HF and their protonated and deprotonated ions and hydrogen-bonded complexes, J. Chem. Theor. Comput. 4 (2008) 967–973.
[58] J.E. Del Bene, I. Alkorta, J. Elguero, Ab initio EOM-CCSD spin − spin coupling constants for hydrogen-bonded formamide complexes: bridging complexes with H_3,$(NH_3)_2$, H_2O,$(H_2O)_2$, FH, and $(FH)_2$, J. Phys. Chem. A 112 (2008) 6338–6343.
[59] J.E. Del Bene, I. Alkorta, I.J. Elguero, Systematic comparison of second-order polarization propagator approximation (SOPPA) and equation-of-motion coupled cluster singles and doubles (EOM-CCSD) spin − spin coupling constants for molecules with C, N, and O double and triple bonds and selected F-substituted derivatives, J. Chem. Theor. Comput. 5 (2009) 208–216.
[60] I. Alkorta, F. Blanco, J. Elguero, A SOPPA theoretical study of the spin–spin coupling constants of all fluorobenzenes $C_6H_nF_{(6-n)}$, n = 0–5, J. Mol. Struct. 964 (2010) 119–125.
[61] O.B. Lutnaes, T.A. Ruden, T. Helgaker, The performance of hybrid density functional theory for the calculation of indirect nuclear spin–spin coupling constants in substituted hydrocarbons, Magn. Reson. Chem. 42 (2004) S117.
[62] R.M. Claramunt, D. Sanz, I. Alkorta, J. Elguero, A theoretical study of multinuclear coupling constants in pyrazoles, J. Magn. Reson. Chem. 43 (2005) 985.
[63] S.N. Maximoff, J.E. Peralta, V. Barone, G.E. Scuseria, Assessment of density functionals for predicting one-bond carbon-hydrogen NMR spin-spin coupling constants, J. Chem. Theor. Comput. 1 (2005) 541.
[64] T.W. Keal, T. Helgaker, P. Salek, D. Tozer, Choice of exchange-correlation functional for computing NMR indirect spin–spin coupling constants, J. Chem. Phys. Lett. 425 (2006) 163.
[65] T.W. Keal, D.J. Tozer, T. Helgaker, GIAO shielding constants and indirect spin–spin coupling constants: performance of density functional methods, Chem. Phys. Lett. 391 (2004) 374–379.
[66] M. Witanowski, K. Kamienska-Trela, Z. Biedrzycka, Indirect carbon–carbon couplings across one, two and three bonds in substituted benzenes: experiment and theory, J. Mol. Struct. 844 (2007) 13.
[67] A.C. Neto, F.P. dos Santos, A.S. Paula, C.F. Tormena, R. Rittner, Density functionals for calculating NMR $^1J_{CH}$ coupling constants in electron-rich systems, Chem. Phys. Lett. 454 (2008) 129.
[68] R. Suardiaz, C. Pérez, R. Crespo-Otero, J.M. Garcia de la Vega, J. San Fabian, Influence of density functionals and basis sets on one-bond carbon-carbon NMR spin-spin coupling constants, J. Chem. Theor. Comput. 4 (2008) 448–456.

[69] L.B. Krivdin, R.H. Contreras, Recent advances in theoretical calculations of indirect spin–spin coupling constants, Annu. Rep. NMR Spectrosc. 61 (2007) 133.
[70] T. Helgaker, M. Jaszunski, M. Pecul, The quantum-chemical calculation of NMR indirect spin–spin coupling constants, Prog. Nucl. Magn. Reson. Spectrosc. 53 (2008) 249.
[71] R.H. Contreras, J.E. Peralta, Angular dependence of spin–spin coupling constants, Prog. Nucl. Magn. Reson. Spectrosc. 37 (2000) 321.
[72] R.H. Contreras, J.E. Peralta, C.G. Giribet, M.C. De Azua, J.C. Facelli, Advances in theoretical and physical aspects of spin-spin coupling constants, Annu. Rep. NMR Spectrosc. 41 (2000) 55.
[73] R.H. Contreras, V. Barone, J.C. Facelli, J.E. Peralta, Advances in theoretical and physical aspects of spin–spin coupling constants, Annu. Rep. NMR Spectrosc. 51 (2003) 167–260.
[74] R.H. Contreras, A.L. Esteban, E. Díez, E.W. Della, I.J. Lochert, F.P. dos Santos, C.F. Tormena, Experimental and theoretical study of hyperconjugative interaction effects on NMR $^{1}J_{CH}$ scalar couplings, J. Phys. Chem. A 110 (2006) 4266.
[75] C.F. Tormena, J.D. Vilcachagua, V. Karcher, R. Rittner, R.H. Contreras, Experimental and theoretical investigation of NMR $^{2}J_{HH}$ coupling constant on six-membered ring systems containing oxygen or sulfur atoms, Magn. Reson. Chem. 45 (2007) 590.
[76] R.H. Contreras, P.F. Provasi, F.P. dos Santos, C.F. Tormena, Stereochemical dependence of NMR geminal spin–spin coupling constants, Magn. Reson. Chem. 47 (2009) 113.
[77] P.R.L. Markwick, R. Sprangers, M. Sattler, Dynamic effects on J-couplings across hydrogen bonds in proteins, J. Am. Chem. Soc. 124 (2003) 644.
[78] P.R.L. Markwick, R. Sprangers, M. Sattler, Dynamic effects on J-couplings across hydrogen bonds in proteins, J. Am. Chem. Soc. 2003 (125) (2003) 644–645, J. Am. Chem. Soc. 129 (2007) 8048.
[79] He Xiao, B. Wang, K.M. Merz Jr., Protein NMR chemical shift calculations based on the automated fragmentation QM/MM approach, J. Phys. Chem. B 113 (2009) 10380–10388.
[80] B. Wang, H. Xiao, K.M. Merz, Quantum mechanical study of vicinal J spin–spin coupling constants for the protein backbone, J Chem Theory Comput 9 (2013) 4653–4659.
[81] J.M. Schmidt, M. Blumel, F. Lohr, H. Ruterjans, Self-consistent ^{3}J coupling analysis for the joint calibration of Karplus coefficients and evaluation of torsion angles, J. Biomol. NMR 14 (1999) 1.
[82] C. Perez, F. Lohr, H. Ruterjans, J.M. Schmidt, Self-consistent Karplus parameterization of ^{3}J couplings depending on the polypeptide side-chain torsion ξ1, J. Am. Chem. Soc. 123 (2001) 7081.
[83] J.M. Schmidt, Asymmetric Karplus curves for the protein side-chain ^{3}J couplings, J. Biomol. NMR 37 (2007) 287.
[84] IUPAC-IUB Commission on Biochemical Nomenclature, J. Mol. Biol. 52 (1970) 1, Biochemistry 9 3471, 3479.
[85] B. Coxon, Developments in the Karplus equation as they relate to the NMR coupling constants of carbohydrates. Advances in carbohydrate chemistry and biochemistry 62 (2009), 17–82.
[86] R. Stenutz, Hetero- and homonuclear coupling constant calculation. Jul 31, 2013, http://www.stenutz.eu/conf/karplus.html.
[87] H. Zhao, Q. Pan, W. Zhang, I. Carmichael, A.S. Serianni, DFT and NMR studies of $^{2}J_{COH}$, $^{3}J_{HCOH}$, and $^{3}J_{CCOH}$ spin-couplings in saccharides: CO torsional bias and H-bonding in aqueous solution, J. Org. Chem. 72 (2007) 7071.
[88] B. Coxon, A Karplus equation for $^{3}J_{HCCN}$ in amino sugar derivatives, Carbohydr. Res. 342 (2007) 1044–1054.
[89] I. Tvaroška, L. Václavík, Stereochemistry of nonreducing disaccharides in solution, Carbohydr. Res. 160 (1987) 137–149.

[90] G.L. Butterfoss, E.F. DeRose, S.A. Gabel, L. Perera, J.M. Krahn, G.A. Mueller, X. Zheng, R.E. London, Conformational dependence of ^{13}C shielding and coupling constants for methionine methyl groups, J. Biomol. NMR 48 (2010) 31–47.
[91] R. Stenutz, I. Carmichael, G. Widmalm, A.S. Serianni, Hydroxymethyl group conformation in saccharides: structural dependencies of 2JHH, 3JHH, and 1JCH spin–spin coupling constants, J. Org. Chem. 67 (2002) 949–958.
[92] C. Thibaudeau, R. Stenutz, B. Hertz, T. Klepach, S. Zhao, Q. Wu, I. Carmichael, A.S. Serianni, Correlated C–C and C–O bond conformations in saccharide hydroxymethyl groups: parameterization and application of redundant ^{1}H–^{1}H, ^{13}C–^{1}H, and ^{13}C–^{13}C NMR J-couplings, J. Am. Chem. Soc. 126 (2004) 15668–15685.
[93] M. Tafazzoli, M. Ghiasi, New Karplus equations for $^{2}J_{HH}$, $^{3}J_{HH}$, $^{2}J_{CH}$, $^{3}J_{CH}$, $^{3}J_{COCH}$, $^{3}J_{CSCH}$, and $^{3}J_{CCCH}$ in some aldohexopyranoside derivatives as determined using NMR spectroscopy and density functional theory calculations, Carbohydr. Res. 342 (2007) 2086–2096.
[94] M. Mobli, A. Almond, N-Acetylated amino sugars: the dependence of NMR $^{3}J(HNH_2)$-couplings on conformation, dynamics, and solvent, Org. Biomol. Chem. 5 (2007) 2243–2251.
[95] H. Zhao, I. Carmichael, A.S. Serianni, Oligosaccharide trans-glycoside 3 J COCC karplus curves are not equivalent: effect of internal electronegative substituents, J. Org. Chem. 73 (2008) 3255–3257.
[96] C. Pérez, R. Suardíaz, P.J. Ortiz, R. Crespo-Otero, G.M. Bonetto, J.A. Gavín, On the unusual $^{2}JC_2H_f$ coupling dependence on syn/anti CHO conformation in 5-X-furan-2-carboxaldehydes, Magn. Reson. Chem. 46 (2008) 846–850.
[97] M.R. Richards, Y. Bai, T.L. Lowary, Comparison between DFT- and NMR-based conformational analysis of methyl galactofuranosides, Carbohydr. Res. 374 (2013) 103–114.
[98] R. Suardiaz, C. Perez, J.M. de la Vega, J. San Fabian, R.H. Contreras, Theoretical Karplus relationships for vicinal coupling constants around $\chi 1$ in valine, Chem. Phys. Lett. 442 (2007) 119.
[99] J.M. García De La Vega, J. San Fabián, R. Crespo-Otero, R. Suardíaz, C. Pérez, Conformational and NMR study of some furan derivatives by DFT methods, Int. J. Quant. Chem. 113 (2013) 656–660.
[100] R.H. Contreras, R. Suardíaz, C. Pérez, R. Crespo-Otero, J. San Fabián, J.M. García de la Vega, Karplus equation for 3 J HH spin − spin couplings with unusual $^{3}J(180°) < {}^{3}J(0°)$ relationship, J Chem Theory Comput 4 (2008) 1494.
[101] R.H. Contreras, R. Suardíaz, C. Pérez, R. Crespo-Otero, J. San Fabián, J.M. García de la Vega, NMR spin–spin coupling constants and hyperconjugative interactions, Int. J. Quant. Chem. 110 (2010) 532.
[102] D.A. Case, C. Scheurer, R. Bruschweiler, Static and dynamic effects on vicinal scalar J couplings in proteins and peptides: a MD/DFT analysis, J. Am. Chem. Soc. 122 (2000) 10390.
[103] A.S. Edison, J.L. Markley, F. Weinhold, Calculations of one-, two-and three-bond nuclear spin-spin couplings in a model peptide and correlations with experimental data, J. Biomol. NMR 4 (1994) 519–542.
[104] A.S. Edison, F. Weinhold, W.M. Westler, J.L. Markley, Estimates of ϕ and ψ torsion angles in proteins from one-, two-and three-bond nuclear spin-spin couplings: application to staphylococcal nuclease, J. Biomol. NMR 4 (1994) 543–551.
[105] M. Hennig, W. Bermel, H. Schwalbe, C. Griesinger, Determination of ψ torsion angle restraints from 3J(Cα, Cα) and 3J(Cα, HN) coupling constants in proteins, J. Am. Chem. Soc. 122 (2000) 6268–6277.
[106] J. Wirmer, H. Schwalbe, Angular dependence of 1J(Ni, Cαi) and 2J(Ni, Cα(i − 1)) coupling constants measured in J-modulated HSQCs, J. Biomol. NMR 23 (2002) 47.

[107] W. Kozminski, I. Zhukov, M. Pecul, J. Sadlej, A protein backbone ψ and φ angle dependence of 2JN(i), Cα(i-1): the new NMR experiment and quantum chemical calculations, J. Biomol. NMR 31 (2005) 87.
[108] E. Puttonen, H. Tossavainen, P. Permi, Simultaneous determination of one- and two-bond scalar and residual dipolar couplings between $^{13}C'$, $^{13}C_\alpha$ and ^{15}N spins in proteins, Magn. Reson. Chem. 44 (2006) S168–S176.
[109] K. Kazimierczuk, A. Zawadzka, W. Kozminski, I. Zhukov, Determination of spin − spin couplings from ultrahigh resolution 3D NMR spectra obtained by optimized random sampling and multidimensional Fourier transformation, J. Am. Chem. Soc. 130 (2008) 5404–5405.
[110] J. Graf, P.H. Nguyen, G. Stock, H. Schwalbe, Structure and dynamics of the homologous series of alanine peptides: a joint molecular dynamics/NMR study, J. Am. Chem. Soc. 129 (2007) 1179–1189.
[111] A. Wu, D. Cremer, A.A. Auer, J. Gauss, Extension of the Karplus relationship for NMR spin-spin coupling constants to nonplanar ring systems: pseudorotation of cyclopentane, J. Phys. Chem. A 106 (2002) 657.
[112] J.B. Houseknecht, T.L. Lowary, C.M. Hadad, Improved Karplus equations for 3JC1, H4 in aldopentofuranosides: application to the conformational preferences of the methyl aldopentofuranosides, J. Phys. Chem. A 107 (2003) 372.
[113] M. Pecul, T. Helgaker, The spin–spin coupling constants in ethane, methanol and methylamine: a comparison of DFT, MCSCF and CCSD results, Int. J. Mol. Sci. 4 (2003) 143.
[114] I. Alkorta, J. Elguero, The influence of chain elongation on Karplus-type relationships: a DFT study of scalar coupling constants in polyacetylene derivatives, Org. Biomol. Chem. 1 (2003) 585.
[115] P.F. Provasi, C.A. Gomez, G.A. Aucar, Hyperconjugation: the electronic mechanism that may underlie the Karplus curve of vicinal NMR indirect spin couplings, J. Phys. Chem. A 108 (2004) 6231.
[116] L.B. Krivdin, Non-empirical calculations of NMR indirect carbon–carbon coupling constants. Part 7-Spiroalkanes, Magn. Reson. Chem. 42 (2004) 500.
[117] I. Alkorta, J. Elguero, Karplus-type relationships between scalar coupling constants: $^{3}J_{HH}$ molecular versus $^{4h}J_{HH}$ supramolecular coupling constants, Theor. Chem. Acc. 111 (2004) 31.
[118] P. Bour, I. Raich, J. Kaminsky, R. Hrbal, J. Cejka, V. Sychrovsky, Restricted conformational flexibility of furanose derivatives: ab initio interpretation of their nuclear spin-spin coupling constants, J. Phys. Chem. A 108 (2004) 6365.
[119] E. Diez, J. Casanueva, J. San Fabian, A. Esteban, M.P. Galache, V. Barone, J.E. Peralta, R.H. Contreras, Prediction of vicinal proton–proton coupling constants $^{3}J_{HH}$ from density functional theory calculations, Mol. Phys. 103 (2005) 1307.
[120] J.E. Del Bene, J. Elguero, Karplus-type equations for $^{1}J(XY)$ in molecules $H_mX\text{-}YH_n$: (X, Y = N, O, P, S), J. Phys. Chem. A 110 (2006) 12543.
[121] J.E. Del Bene, J. Elguero, Variation of one-bond XY coupling constants $^{1}J(XY)$ and the components of $^{1}J(XY)$ with rotation about the XY bond for molecules $H_mX\text{-}YH_n$, with X, Y = ^{15}N, ^{17}O, ^{31}P, ^{33}S: the importance of nonbonding pairs of electrons, J. Phys. Chem. A 111 (2007) 2517–2526.
[122] G. Palermo, R. Riccio, G. Bifulco, Effect of electronegative substituents and angular dependence on the heteronuclear spin − spin coupling constant $^{3}J_{C-H}$: an empirical prediction equation derived by density functional theory calculations, J. Org. Chem. 75 (2010) 1982–1991.
[123] P. Salvador, I.-H. Tsai, J.J. Dannenberg, J-coupling constants for a trialanine peptide as a function of dihedral angles calculated by density functional theory over the full Ramachandran space, Phys. Chem. Chem. Phys. 13 (2011) 17484–17493.

[124] N. Juranic, J.J. Dannenberg, G. Cornilescu, P. Salvador, E. Atanasova, H.-C. Ahn, S. Macura, J.L. Markley, F.G. Prendergast, Structural dependencies of protein backbone $^{2}J_{NC'}$ couplings, Protein Sci. 17 (2008) 768.
[125] Y.Y. Rusakov, L.B. Krivdin, Modern quantum chemical methods for calculating spin–spin coupling constants: theoretical basis and structural applications in chemistry, Russ. Chem. Rev. 82 (2013) 99.
[126] J.M. Schmidt, M.J. Howard, M. Maestre-Martínez, C.S. Pérez, F. Löhr, Variation in protein C_{α}-related one-bond J couplings, Magn. Reson. Chem. 47 (2009) 16–30.
[127] J.M. Schmidt, Y. Hua, F. Löhr, Correlation of ^{2}J couplings with protein secondary structure, Proteins 78 (2010) 1544–1562.
[128] M.I.-H. Tsai, Y. Xu, J.J. Dannenberg, Ramachandran revisited. DFT energy surfaces of diastereomeric trialanine peptides in the gas phase and aqueous solution, J. Phys. Chem. B 113 (2009) 309.
[129] J.-S. Hu, A. Bax, Measurement of three-bond 13C-13C J couplings between carbonyl and carbonyl/carboxyl carbons in isotopically enriched proteins, J. Am. Chem. Soc. 118 (1996) 8170.
[130] J.-S. Hu, A. Bax, Determination of ϕ and ξ1 angles in proteins from ^{13}C-^{13}C three-bond J couplings measured by three-dimensional heteronuclear NMR. How planar is the peptide bond? J. Am. Chem. Soc. 119 (1997) 6360.
[131] N. Juranic, E. Atanasova, M.C. Moncrieffe, F.G. Prendergast, S. Macura, Calcium-binding proteins afford calibration of dihedral-angle dependence of $^{3}J_{NC\gamma}$ coupling constant in aspartate and asparagine residues, J. Magn. Reson. 175 (2005) 222.
[132] S. Vijay-Kumar, C.E. Bugg, W.J. Cook, Structure of ubiquitin refined at 1.8Å resolution, J. Mol. Biol. 194 (1987) 531–544.
[133] A.C. Wang, A. Bax, Reparameterization of the Karplus relation for $^{3}J(H_{\alpha}$-N) and $^{3}J(H_N$-C') in peptides from uniformly $^{13}C/^{15}N$-enriched human ubiquitin, J. Am. Chem. Soc. 1995 (1810) 117.
[134] K. Ding, A.M. Gronenborn, Protein backbone $^{1}H_N$-$^{13}C_{\alpha}$ and ^{15}N-$^{13}C_{\alpha}$ residual dipolar and J couplings: new constraints for NMR structure determination, J. Am. Chem. Soc. 126 (2004) 6232.